



Retreat and stabilization of a marine-based ice margin along a high arctic fjord-cross-shelf trough system



Pierre-Olivier Couette ^{a,b,*}, Patrick Lajeunesse ^a, Jean-François Ghienne ^b, Boris Dorschel ^c, Catalina Gebhardt ^c, Dierk Hebbeln ^d, Etienne Brouard ^{e,f}

^a Département de Géographie, Université Laval, Québec, Canada

^b Institut Terre Environnement de Strasbourg (ITES), UMR 7063, CNRS—Université de Strasbourg, Strasbourg, France

^c Alfred-Wegener-Institut Helmholtz-Zentrum für Polar- und Meeresforschung (AWI), Bremerhaven, Germany

^d MARUM, Center for Marine Environmental Sciences, University of Bremen, Bremen, Germany

^e Département des Sciences de la Terre et de l'atmosphère & GEOTOP, Université du Québec à Montréal, Canada

^f Geological Survey of Canada, Natural Resources Canada, Ottawa, Canada

ARTICLE INFO

Article history:

Received 16 July 2022

Received in revised form

21 December 2022

Accepted 28 December 2022

Available online 17 January 2023

Handling editor: A. Voelker

Keywords:

Laurentide Ice Sheet

Baffin Island

Deglaciation

Holocene

Submarine landforms

Marine sediment cores

Abrupt climatic events

ABSTRACT

Multibeam bathymetric and seismostratigraphic data collected in the Clyde fjord-cross-shelf trough system (eastern Baffin Island, Canadian Arctic Archipelago) display glacial landforms and depositional assemblages that enable the identification of the maximal extent of the Laurentide Ice Sheet (LIS) margin and delineating the patterns and controls on its subsequent retreat. Additionally, 10 new sediment cores – from which seven radiocarbon ages were acquired – allow the recognition of depositional processes. Results show that, during the Last Glacial Maximum, the LIS margin extended almost to the edge of the continental shelf. Early deglaciation of the trough was marked by an initial ice-shelf collapse and rapid retreat of the ice stream, as evidenced by the absence of ice marginal landforms and the presence of extensive iceberg ploughmarks across a large portion of the outer trough. It was followed by a slow retreat and successive stabilizations of the ice margin that led to the deposition of recessional moraines and grounding-zone wedges (GZWs). Deglaciation of the fjord in the early Holocene occurred in an episodic style, whereby rapid retreat was punctuated by relatively long standstills that enabled major moraine formation. Long-term stabilizations of the ice margin in the Clyde fjord-cross-shelf trough system are interpreted to coincide with major climatic cooling events, such as the Younger Dryas and early Holocene cold reversals. Ages derived from sediment cores and previous work suggest that higher retreat rates correspond with periods of significant global sea level rise, suggesting that oceanic forcing exerted a minor control on the deglaciation. GZWs and large moraine ridges are observed at pinning points in the trough and fjord, indicating that the location of ice margin stabilizations was influenced by topography. The reconstruction of the deglaciation of the Clyde fjord-cross-shelf trough system allows us to refine deglacial models for similar systems of northeastern Baffin Island, in particular beyond the coast and along the steeper section of the fjord where chronological gaps remained.

© 2023 Elsevier Ltd. All rights reserved.

1. Introduction

Reconstructing the history of past ice sheets allows to document their inter-relationship with the climate system, especially by providing boundary conditions to test models that aim to simulate climate and ice sheet evolution (Joughin et al., 2012; Stocker et al.,

2013; Rasmussen et al., 2014; Tinto et al., 2019; Briner et al., 2020; Lowry et al., 2020). Past marine-based ice sheet margins such as those of the Laurentide Ice Sheet (LIS) – which was in contact with the western Atlantic Ocean during the Last Glacial Maximum (LGM; ~24 ka BP) – are believed to have operated in a comparable way to the present Antarctic Ice Sheet, with a network of ice streams channeled in bathymetric troughs and mass loss dominated by calving (Ottesen et al., 2005; De Angelis and Kleman, 2007; Margold et al., 2018). Reconstructing palaeo-ice sheet dynamics and deglaciation patterns is therefore fundamental for

* Corresponding author. Département de Géographie, Université Laval, Québec, Canada

E-mail address: pierre-olivier.couette.1@ulaval.ca (P.-O. Couette).

understanding the long-term behaviour of modern ice sheets (i.e., Antarctica and Greenland) and their interconnection with global climate (i.e., Danielson and Bart, 2019; Stokes et al., 2012; Briner et al., 2020; Young et al., 2020, 2021).

Controls and ice-retreat patterns during the deglaciation that followed the LGM still remain poorly documented in the eastern Canadian Arctic Archipelago (CAA) compared to other deglaciated regions of the Northern Hemisphere, such as Norway (e.g., Lyså and Vorren, 1997; Aarseth et al., 1997; Laberg et al., 2009; Bjarnadóttir et al., 2012;), Svalbard (e.g., Winsborrow et al., 2010; Streuff et al., 2018; Flink and Noormets, 2018; Howe et al., 2019; Allaart et al., 2020) and the British Isles (e.g., Arosio et al., 2018; Callard et al., 2020). Off Baffin Island, marine geophysical data suggest that ice retreat was punctuated by successive stabilizations of the late glacial ice margin on the continental shelf (Brouard and Lajeunesse, 2017), while onshore data suggest a rapid ice decay into the fjords during the early Holocene (Miller et al., 2005; Briner et al., 2005, 2007, 2009a; Young et al., 2015; Margreth et al., 2017). However, recent offshore investigations show that multiple ice-margin stabilizations occurred within the fjords of northeastern Baffin Island during the last deglaciation (Brouard and Lajeunesse, 2019a). Stabilizations both on the shelf and in the fjords of northeastern Baffin Island were found to be strongly influenced by bed geometry (Brouard and Lajeunesse, 2017, 2019a), similarly to observations made in other deglaciated fjords and continental shelves (i.e., Aarseth et al., 1997; Hodgson et al., 2014; Batchelor et al., 2019a). These contrasting patterns of ice retreat, which probably arise from the scarcity of valuable data from the submarine domain, complicate the establishment of a reliable model of deglaciation and outline the need for improved understanding of LIS extent and retreat patterns in the fjord-cross-shelf trough systems of Baffin Island by bridging submarine and continental data.

Here we map and analyse submarine landforms and sediment assemblages in the 180 km-long Clyde fjord-cross-shelf trough system, with the aim of refining our understanding of the retreat patterns of the marine-based margin of the northeastern LIS. By using a combination of multibeam bathymetric data, acoustic and seismic profiles as well as sediment cores, the key objectives are to 1) define a chronology for the deglaciation of the LIS in the region; 2) reconstruct changes in the morpho-sedimentary system and dynamics on the shelf and in the fjord; and 3) identify the factors that controlled ice margin retreat rates and stabilization during deglaciation.

2. Regional setting

2.1. Study area

The studied area comprises the fjord of Clyde Inlet and its offshore extension across the continental shelf, namely Clyde Trough (Fig. 1). This fjord-cross-shelf trough system stretches from the interior plateau of Baffin Island to the shelf break facing Baffin Bay.

The continental shelf off Clyde Inlet is generally shallow (<200 m) with a deeper trough carved by repeated occupation by ice streams during Quaternary glaciations (Løken and Hodgson, 1971; Praeg et al., 2007). Precambrian crystalline rocks extend halfway across the continental shelf, where they are overlain by upper Cretaceous-Tertiary strata of the Baffin Bay Basin (Jackson et al., 1984; Fader et al., 1989; Praeg et al., 2007). Clyde Trough is 20–30 km-wide, extends from SW to NE on >60 km, and bends slightly toward the east near the shelf break. Existing coarse resolution bathymetry data (GEBCO) show that the trough is flat-bottomed and has a reverse-gradient slope (Fig. 1C), characteristic of troughs in formerly glaciated areas (Ottesen et al., 2007; Slabon

et al., 2016; Arndt et al., 2017; Bart et al., 2017; Brouard and Lajeunesse, 2017), with water depths decreasing seaward from ~375 m at the mouth of the fjord to ~150 m at the shelf break.

Clyde Inlet is a fjord that has been glacially incised into the Precambrian crystalline rocks of the eastern coastal mountains of Baffin Island during Quaternary glaciations (Jackson et al., 1984; Kleman et al., 2010). With its U-shaped profile and a succession of deep basins separated by intervening sills, it has a typical mid- and high-latitude fjord morphology (Syvitski and Shaw, 1995). Clyde Inlet is 120 km-long, between 3 and 20 km-wide and consist of basins between 200 and 500 m-deep (Fig. 1C). Many hanging valleys of various widths and depths drain into Clyde Inlet, providing localized sediment input through proglacial rivers. Inugsuitt Fjord, a 100 km-long fjord, and Patricia Bay also merge into Clyde Inlet near its mouth. Clyde Inlet is directly connected to the cross-shelf trough, forming a 180 km-long submarine glacial valley system connecting Baffin Island to Baffin Bay and separated by a shallow bedrock sill at the fjord mouth.

Most of the valleys, lowlands, fjords and trough of Clyde Inlet and nearby areas are covered by a thick sequence of Quaternary deposits (Jackson et al., 1984; Praeg et al., 2007; Brouard and Lajeunesse, 2017, 2019a, 2019b).

2.2. Late Quaternary glacial history

Late Wisconsinan (MIS 2) ice sheets started building up at ~28 ka BP (Stokes et al., 2012; Kleman et al., 2010; Batchelor et al., 2019b) and reached their maximal extent by 24 ka BP in many sectors of North America (Dyke et al., 2002; Andrews and Dyke, 2007; Hughes et al., 2013). Although many models have been proposed for establishing the maximal extent of the LIS at the LGM, recent studies indicate that the ice margin extended at or near the edge of the northeastern Baffin Island shelf (Briner et al., 2006; Li et al., 2011; Brouard and Lajeunesse, 2017; Jenner et al., 2018; Dalton et al., 2020; Lévesque et al., 2020; Couette et al., 2022). In between the fjords, cosmogenic exposure dating on glacial erratics and bedrock suggest an extensive LIS cover during the LGM (Briner et al., 2005; Davis et al., 2006). Marine geophysical data also show that an ice shelf covered northern Baffin Bay during the LGM, possibly buttressing peripheral ice streams and impacting their flow to the ocean (Couette et al., 2022).

Following the LGM, the break up of the Baffin Bay ice shelf between 16 and 14.6 ka BP provoked a major reorganization of the ice-sheet drainage system by removing the buttressing effect on ice streams (Couette et al., 2022), and therefore led to ice-flow acceleration in systems from northeastern Baffin Island (Jenner et al., 2018). This event was found to be more or less coeval with the deposition of a detrital carbonate sediment layer in Baffin Bay (BBDC-1), corresponding to massive ice discharge from ice streams of the CAA and northwest Greenland and characterized by Ca-rich sediments (Hiscott et al., 1989; Andrews et al., 1998; Simon et al., 2014; Jackson et al., 2017; Jenner et al., 2018). This iceberg discharge event was followed by a period of important ice retreat on the shelf off eastern Baffin Island coinciding with the Bølling-Allerød warm period (Dyke et al., 2002; Briner et al., 2005; Margreth et al., 2017; Brouard and Lajeunesse, 2017; Jenner et al., 2018). The subsequent retreat towards Baffin Island mainland was punctuated by glacier readvances or stabilizations during the cold phase of the Younger Dryas (12.9–11.7 ka BP) which led to the building of major moraine systems (Briner et al., 2007; Margreth et al., 2017; Young et al., 2020). Following the Younger Dryas, and under the warmer climate of the early Holocene period, the ice margin retreated rapidly to reach the inner fjord (Andrews and Ives, 1978; Briner et al., 2007, 2009b). This rapid ice-margin retreat was temporarily interrupted by ice-margin stabilizations during short

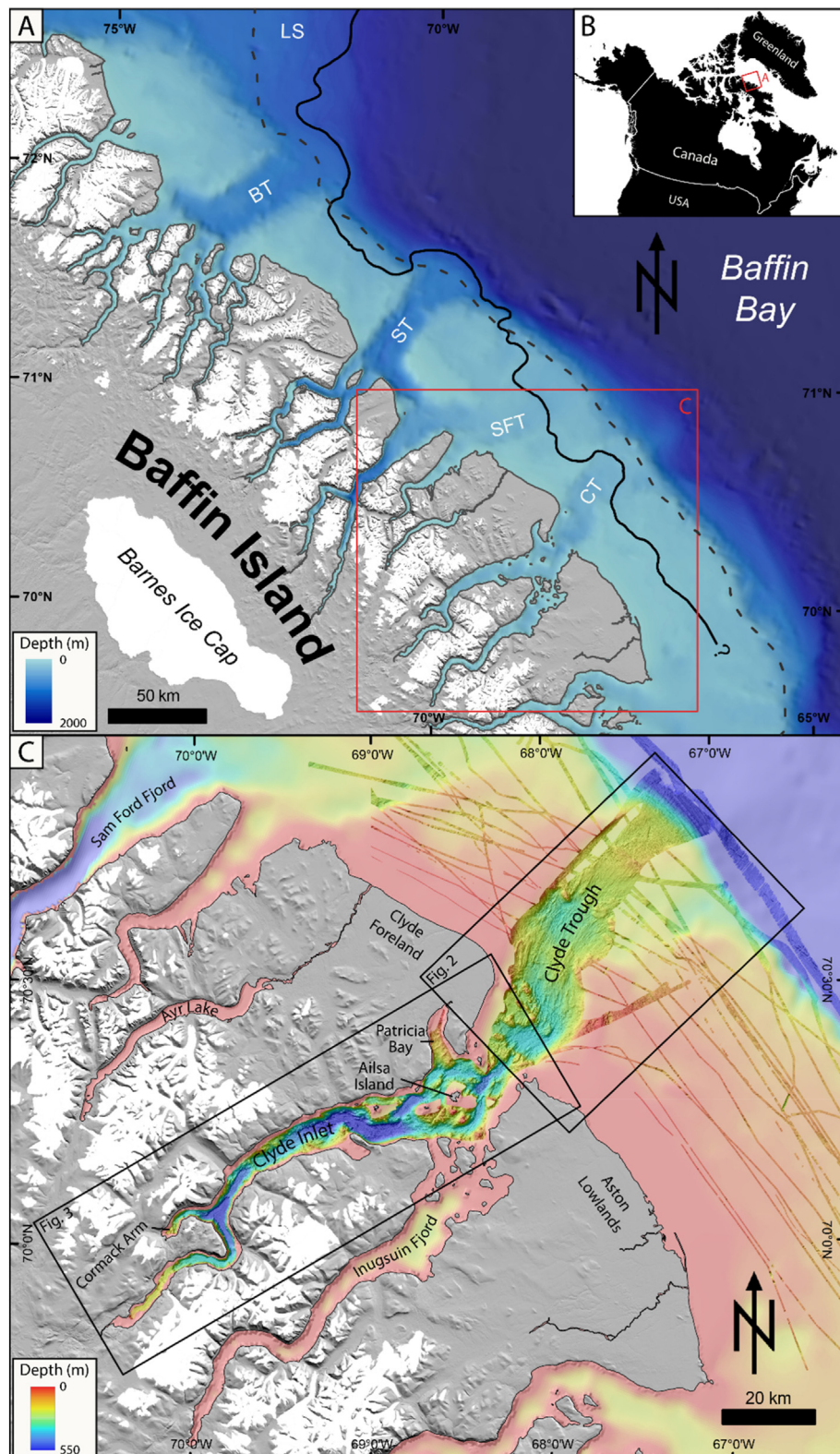


Fig. 1. (A) Baffin Bay and the proposed LGM limit on northeastern Baffin Island, modified from [Brouard and Lajeunesse \(2017\)](#). LS: Lancaster Sound; BT: Buchan Trough; ST: Scott Trough; SFT: Sam Ford Trough; CT: Clyde Trough. The dashed line represents the LIS extent at the LGM from [Dalton et al. \(2020\)](#). (B) Location of the study area. (C) Map showing the multibeam bathymetric data used in this study draped on the International Bathymetric Chart of the Arctic Ocean data gridded at a 500 m cell-size resolution (IBCAO; [Jakobsson et al., 2014](#)). The hillshade is from the Canadian Digital Elevation model (CDEM).

cold events at 10.3, 9.3 and 8.2 ka (Briner et al., 2007, 2009b; Young et al., 2012, 2020; Crump et al., 2020). The latter event is recorded at the fjord heads on eastern Baffin Island and referred to as the Cockburn stage moraine (Andrews and Ives, 1978; Briner et al., 2007, 2009b; Brouard and Lajeunesse, 2019a; Young et al., 2021). Subsequently, the LIS margin retreated steadily from the fjord head and separated to form what are today's Barnes and Penny ice caps (Dyke, 2004; Miller et al., 2005; Briner et al., 2009b).

3. Material and methods

This study is based on the integration of multibeam bathymetric, shallow acoustic, seismic and sediment core data. The main bathymetric dataset was acquired during expedition MSM66 of the German research vessel RV Maria S. Merian in August 2017 (Dorschel et al., 2017). The MSM66 data are complemented by bathymetric data collected during ArcticNet cruises onboard the CCGS Amundsen (2003–2017). Shallow acoustic data and sediment cores were also collected during MSM66 (Dorschel et al., 2017). Seismic data were acquired by the Geological Survey of Canada during airgun surveys in 1978 and 1980.

3.1. Multibeam bathymetric data

MSM66 bathymetric data were collected with a Kongsberg Simrad EM122 (12 kHz) multibeam echosounder (MBES), while the CCGS Amundsen data were collected with a Kongsberg Simrad EM302 (30 kHz) MBES. These datasets were processed for anomalous data points and artefacts removal using Caris Hips and Sips software. The datasets were gridded with a 10 m cell-size resolution and then imported into ESRI ArcGIS 10.8 software for geomorphological mapping and interpretation.

3.2. Shallow acoustic and seismic data

Shallow acoustic data were recorded with an Atlas Parasound DS P-70 system (5–33 kHz) during MSM66. The raw data were recorded into PS3 format and then converted into SEGY using ps32seg3 software of Dr. Hanno Keil (University of Bremen). The acoustic profiles were then imported into the SMT Kingdom Suite software for processing and interpretation.

Seismic lines 78029_AG_275_0130 and 80028_AG_RAYT_257_0200 were acquired on expeditions 78029 (1978) and 80028 (1980) by Brian MacLean of the Geological Survey of Canada-Atlantic (Cruise reports available via https://ed.marine-geo.ca/cruise_report_e.php). Extraction and interpretation was performed using the LizardTech GeoViewer software. Both acoustic and seismic data were transferred into Adobe Illustrator for figure production. Thicknesses and water depth were calculated using a velocity of 1500 m/s.

3.3. Core data

The sediment cores collected during expedition MSM66 were between 137 and 965 cm long (Table 1). On board, all cores were split, visually described with a particular focus on noting the lithology, texture, contacts, sedimentary structures and Munsell color, as well as digitally photographed.

X-ray fluorescence (XRF) scanning were used to characterize elemental properties of the sediments by using a XRF Core Scanner II (AVAATECH Serial No. 2) at MARUM, University of Bremen. Data were collected every 2 cm down-core over a 15 mm² area with down-core slit size of 10 mm using generator settings of 10 kV, a current of 0.2 mA and a sampling time of 10 s directly at the split core surface of the archive half. The split core surface was covered

Table 1

Information on cores collected in the Clyde fjord-cross-shelf trough system.

Core name	Latitude	Longitude	Water depth (m)	Core length (cm)
GeoB22344-3	70°03.90'N	70°02.93'W	367	483
GeoB22346-3	69°54.18'N	70°13.54'W	203	783
GeoB22348-3	69°58.47'N	69°57.47'W	362	896
GeoB22350-3	70°08.52'N	69°44.36'W	435	137
GeoB22351-3	70°10.16'N	69°38.30'W	364	523
GeoB22353-3	70°13.35'N	69°00.16'W	489	862
GeoB22356-3	70°27.68'N	67°58.36'W	338	965
GeoB22357-3	70°36.28'N	67°53.63'W	315	902
GeoB22358-3	70°41.69'N	67°41.83'W	261	500
GeoB22359-3	70°46.06'N	67°27.96'W	196	166

with a 4 µm thin SPEXcerti Prep Ultralene1 foil to avoid contamination of the XRF measurement unit and desiccation of the sediment. Raw spectra data were processed by the analysis of X-ray spectra in the Iterative Least square software (WIN AXIL) package from Canberra Eurisy.

Accelerator Mass Spectrometry (AMS) radiocarbon dating was carried out on benthic foraminifera assemblages and shell fragments. Samples were sent to the MICADAS-laboratory (Alfred Wegener Institute, Bremerhaven), where CO₂ from small amount of foraminiferal carbonate (~0.5 mg) were analysed. Additionally, three dates based on shell fragments were obtained. The AMS ¹⁴C ages were converted to calendar years before present (cal. BP) using the online software Calib 8.2 with the Marine20 radiocarbon age calibration curve (Heaton et al., 2020). The Marine20 calibration curve uses a global marine reservoir age that is not suitable for the polar regions, an issue that requires the application of additional reservoir correction (ΔR) values to high-latitudes samples (Heaton et al., 2020). Therefore, an additional local ΔR of 81 ± 18 was used to account for the regional offset of the world ocean ¹⁴C age (Pieńkowski et al., 2022). The ΔR value is kept constant for the entire period, although we acknowledge that oceanographic conditions such as circulation, ventilation and extensive sea-ice cover during glacial periods may result in the overestimation of the actual calendar ages (Heaton et al., 2022; Pieńkowski et al., 2022). However, as our ages are from the early Holocene, they were likely little affected by such changes in oceanographic conditions. We argue that using only an additional local reservoir correction therefore provides an appropriate estimate for these ages, with relatively minimal uncertainties.

4. Results

4.1. Seafloor geomorphology

Complete multibeam bathymetric coverage of the Clyde fjord-cross-shelf trough system allowed identifying several submarine glacial landforms (Figs. 2 and 3) that are here described and interpreted for reconstructing the past configuration, stages and dynamics of the LIS margin. Figs. 4 and 5.

4.1.1. Subglacial landforms

Several streamlined landforms oriented along the fjord and trough axis are observed in the Clyde fjord-cross-shelf trough system and represent variations in ice-flow direction and velocity. They are here grouped under the generic term glacial lineations.

Glacial lineations - Sets of streamlined and curvilinear ridges oriented parallel to the trough axis are observed at depths between 100 m and 500 m; they are up to 5 km-long (Figs. 4, 5A and 5C, 6A and 6D). These streamlined landforms are between 50 m and 500 m-wide and can be as much as 60 m-high compared to the surrounding seafloor. These ridges are mostly aligned parallel to

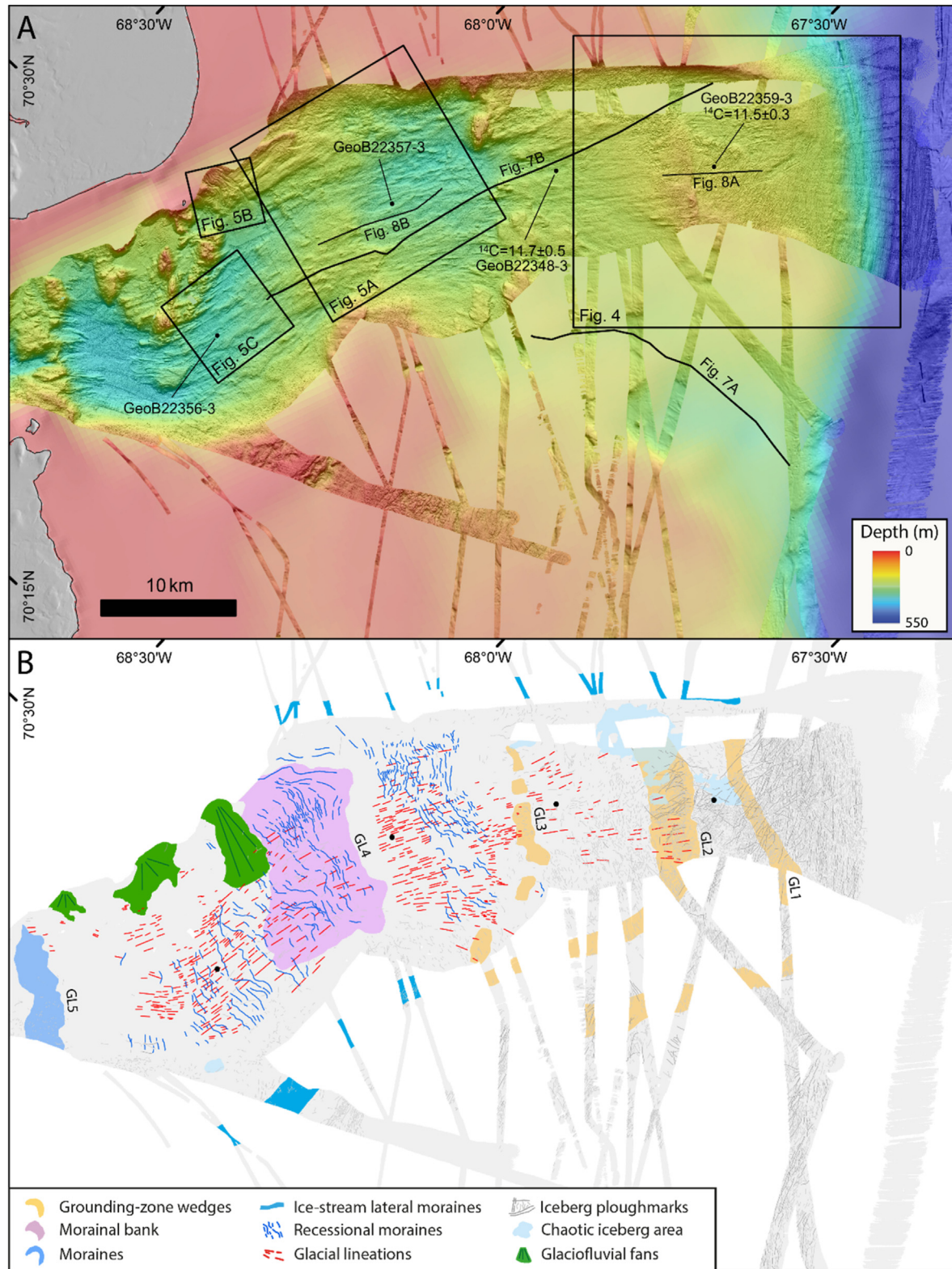


Fig. 2. (A) Multibeam bathymetry of Clyde Trough. Boxes show the location of Figs. 4 and 5. Dashed brown lines represent moraine ridges from Briner et al. (2007). Ages derived from the sediment cores represent minimum age for deglaciation at the core site. (B) The mapped distribution of submarine landforms in the trough.

each others, but are in some cases divergent where the trough widens. Features with lower length to width ratios (between 1:5 and 1:20) tend to be asymmetrical, with a gentler seaward slope, and occur mostly beyond bedrock outcrops. Conversely, ridges with

higher length to width ratios (up to 1:50) are more symmetrical, subtle and tend to have a smoother appearance. These ridges are in some cases superimposed on grounding line landforms.

These streamlined landforms are interpreted as glacial

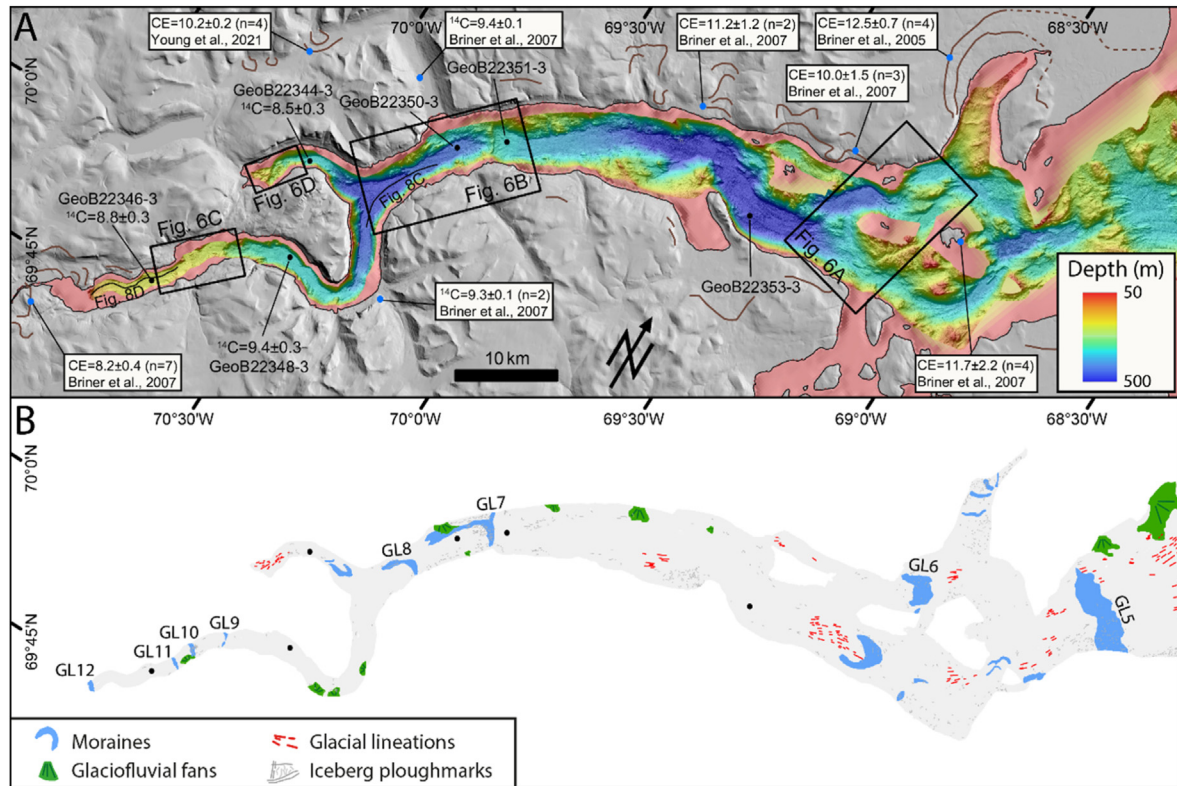


Fig. 3. (A) Bathymetry of Clyde Inlet. Boxes show the location of Fig. 6A–D. Brown lines represent moraine ridges from Briner et al. (2007). Ages derived from the sediment cores represent minimum age for deglaciation at the core site. Blue dots indicate cosmogenic exposure (CE) and radiocarbon (^{14}C) dating discussed in the text, compiled from previous studies along Clyde Inlet (in ka ± 1 SD uncertainties). (B) The mapped distribution of submarine landforms in the fjord.

lineations, such as mega-scale glacial lineations (MSGUs), drumlins and crag-and-tails, which provide evidence for former ice-flow directions as they are parallel to another (Clark, 1993; Stokes and Clark, 2001; Spagnolo et al., 2014; Dowdeswell et al., 2016a; Maclean et al., 2016; Batchelor et al., 2018; Ottesen et al., 2022). Glacial lineations are differentiated on the basis of their width to length ratio and their formation processes. MSGUs are generally highly elongated (up to 1:50 length to width ratio) and are produced by the deformation of soft till beneath a fast-flowing ice stream (e.g., Clark, 1993) or as a product of ice keels ploughing through sediments (e.g., Tulaczyk et al., 2001; Clark et al., 2003). In turn, crag-and-tails and drumlins are less elongated (between 1:5 and 1:20 length to width ratio) and formed by the accumulation of sediments on the seaward side of bedrock obstacles or the streamlining of bedrock by ice (Stokes and Clark, 2001; Ottesen et al., 2007). The position of most crag-and-tails beyond bedrock in Clyde Inlet suggests that they were formed by the streamlining action of warm-based ice (Dowdeswell et al., 2016a; Maclean et al., 2016).

4.1.2. Ice marginal landforms

Several sediment wedges and ridges are observed on the multibeam bathymetry imagery and record the extent and retreat pattern of the LIS during the LGM and the deglaciation. GZWs, morainal bank, and end moraines represent major grounding line landforms (referred to as GL in Figs. 2–3 and in the discussion) that record former, successive position of the ice margin along the Clyde fjord-cross-shelf trough system.

Grounding-zone wedges (GZWs) – Asymmetric transverse wedges characterized by steeper ice-distal slope are identified in the outer and middle part of Clyde Trough (Figs. 4 and 7). These

wedges are present at water depths ranging from 150 m to 350 m, have lengths between 3 and 10 km and rise from 20 to 50 m above the surrounding seafloor. On the seismic data, they correspond to wedge-like deposits reaching 15–20 m in thickness and 5 km in length (Fig. 7) with low-reflectivity, transparent and sometimes chaotic acoustic signature. Smooth and gently sloping fan-shaped surfaces (between 0.5 and 2°) are usually identified on the sea-floor in front of those large transverse wedges.

Due to their asymmetric geometry and steep ice-distal slopes, these asymmetric wedges are interpreted as grounding-zone wedges similar to ice-contact wedges reported on other deglaciated continental shelves (e.g., Ottesen et al., 2007, 2022; Slabon et al., 2016; Brouard and Lajeunesse, 2017). Large GZWs are formed during relatively long-term ice margin stabilizations (decadal-to centennial-scale) which enable subglacial sediment accumulation at the grounding line (Powell and Domack, 1995; Dowdeswell and Fugelli, 2012; Batchelor and Dowdeswell, 2015; Dowdeswell et al., 2016b). The accumulation of sediment is interpreted to be vertically limited by the presence of a floating ice shelf seaward from the grounded ice, thus favoring horizontal progradation of sediments and forming low-amplitude extensive wedges (Dowdeswell and Fugelli, 2012; Batchelor and Dowdeswell, 2015; Dowdeswell et al., 2016b). The fan-shaped surfaces are interpreted as ice-marginal debris flow lobes deposited by sediment delivery at the grounding line of a marine terminating glacier (Syvitski and Shaw, 1995; Ó Cofaigh and Dowdeswell, 2001; Bjarnadóttir et al., 2012; Batchelor and Dowdeswell, 2015; Dowdeswell et al., 2015; Ottesen et al., 2017).

Morainal banks – A large asymmetric wedge with a steeper ice-distal side and overprinted by transverse zigzag-shaped ridges and recessional moraines is located in the center of Clyde Trough at a

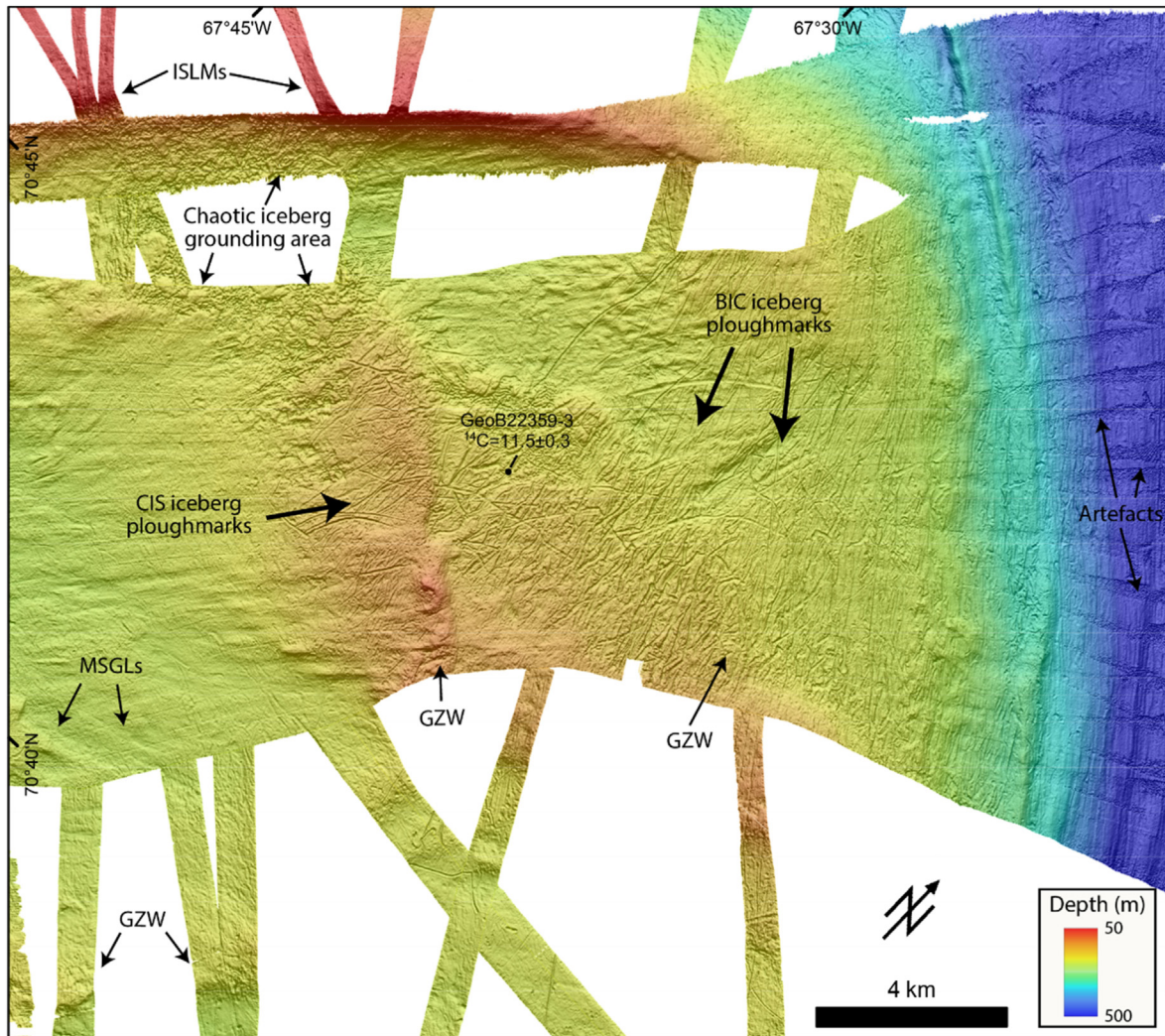


Fig. 4. Multibeam bathymetry of submarine landforms in the outer trough. CIS – Clyde Ice Stream and BIC – Baffin Island Current. For further interpretation and discussion, see Couette et al. (2022).

depth of 325 m (Figs. 5A and 7B). The wedge is 75 m-high, 6 km-long and 12 km-wide, while the overprinting zigzag-shaped ridges are 5–10 m-high, 100 to 200 m-long and between 500 and 1000 m-wide (Fig. 5A). The seismic data show three distinct morphosedimentary units composing the underlying sediment body: (1) a bottom unit showing evidence of glaciotectonism including folds and thrust sheets; (2) an upper unit showing seaward dipping reflectors; and 3) ridges with a chaotic acoustic signature located on the stoss side of the system (Fig. 7B). Gently sloping fan-shaped surfaces are identified in front of this large asymmetric wedge. The associated deposits attenuate underlying landforms such as glacial lineations and recessional moraines (Fig. 5A).

Based on its morphology and the overprinted zigzag-shaped ridges, this landform is interpreted as a morainal bank. Morainal banks are generally associated with a quasi-stagnant ice margin position during overall deglaciation, coherent with the presence of recessional moraines (Powell, 1981; Clark et al., 2003; Laberg et al., 2009; Dowdeswell et al., 2015). Zigzag-shaped ridges are, in turn, associated with sediment deformation related to push and thrust of ice proximal deposits by glacier readvances (Powell, 1981; Clark et al., 2003; Laberg et al., 2009). They could also represent crevasse-squeeze ridges, produced subglacially by basal till being squeezed into crevasses at the glacier bed during an ice advance

(Evans and Rea, 1999; Ottesen et al., 2022). The complex acoustic signature with folds and thrust sheets observed on the seismic profile (Fig. 7B) further support the interpretation of a readvance of the ice margin that lead to the formation of the morainal bank (Laberg et al., 2009). The fan-shaped surfaces observed in front of the morainal bank are interpreted as ice-marginal debris flow lobes (Svititski and Shaw, 1995; Ottesen et al., 2017).

Major end moraines - Arcuate asymmetrical ridges with a steeper ice-proximal slope are observed at several locations along Clyde Inlet (Fig. 6B–C). These landforms range between 10 m and 150 m in height, and between 1 km and 6 km in width. They are 500 m to 3 km-long and are observed at depths reaching 450 m. On the distal flank, fan-shaped surfaces occasionally emanate from the ridges over distances of several kilometers. Ridges located in Patricia Bay have a more subtle and smoother appearance (Fig. 3). Partially buried transverse ridges with steep-scars are also observed at a few locations in the fjord, where they bound step-like basins (Fig. 6B–C). Several linear ridges running parallel to the fjord axis and specifically located on the flanks of the fjord are also observed in Clyde Inlet (Fig. 6B). These ridges are 500 m to 3 km-long, 100 m to 500 m-wide, up to 100 m-high and appear to be, in some cases, the lateral extension of the arcuate ridges (Figs. 5A and 6B).

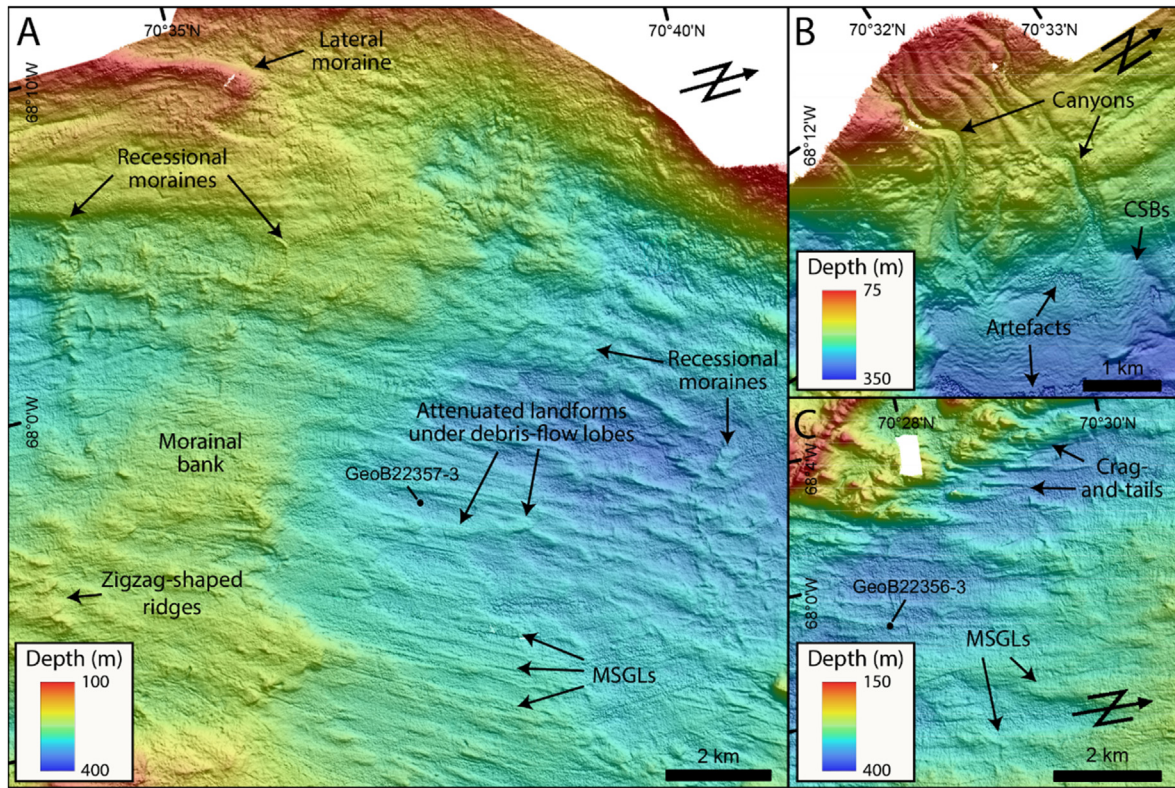


Fig. 5. (A) Multibeam bathymetry of submarine landforms in the middle trough. (B) Glaciofluvial fan, with associated canyons and crescent-shaped bedforms (CSBs), in the middle trough. (C) Mega-scale glacial lineations (MSGLs) in the inner trough.

Due to their geometry and their position transverse to the fjord axis, the arcuate ridges are interpreted as major end moraines, whereas the linear and parallel-to-the-fjord morphologies are, in turn, interpreted as lateral moraines (Dowdeswell and Vásquez, 2013; Dowdeswell et al., 2014; Hodgson et al., 2014). Major end moraines are formed by the deposition and pushing of sediment during long-term ice margin stabilizations of at least decades to centuries (Powell and Alley, 1997; Dowdeswell et al., 2014; Batchelor et al., 2018). In contrast to GZWs, moraine ridges usually develop at the margin of tidewater glacier that have vertically unrestricted accommodation space at the grounding line (Powell and Alley, 1997). Similarly to observations in front of GZWs and the morainal bank, the fan-shaped surfaces are inferred to be ice-marginal debris flow lobes (Svitshi and Shaw, 1995; Ottesen et al., 2017). The moraine ridges in Patricia Bay probably represent deposition by a secondary ice flow across the bay and onto the Clyde forelands (Briner et al., 2005). The step-like basins observed in the fjord are interpreted to be the result of high sediment deposition from transverse deltas fed by nearby rivers and overfilling some of the basins confined by a succession of receding moraines (Hodgson et al., 2014; Brouard and Lajeunesse, 2019a).

Recessional moraines - Small ridges transverse to the former ice flow are specifically identified on the multibeam bathymetric data of the trough (Fig. 5A). They are observed in the mid-to inner section of the trough in water depths ranging from 200 m to 300 m; their size varies between 2 m and 12 m-high and 100 m to 500 m-wide. Some of them can be traced for lengths of >5 km, although the majority do not exceed 1 km. Most of the ridges are arcuate and symmetric. They occur in two distinct clusters of parallel to sub-parallel features spaced a few hundred meters apart.

These small parallel ridges are interpreted as recessional moraines, formed by the delivery and pushing of subglacial sediments

by minor stillstands or readvances of the grounded glacier front in subaqueous conditions (Boulton, 1986; Lindén and Möller, 2005; Dowdeswell et al., 2008; Ó Cofaigh et al., 2008; Arndt et al., 2017; Batchelor et al., 2018; Howe et al., 2019; Ottesen et al., 2022). The presence of recessional moraines in marine environments is usually associated with a relatively slow retreat of the ice margin in water typically shallower than 350 m (Lindén and Möller, 2005; Dowdeswell et al., 2008; Ó Cofaigh et al., 2008; Howe et al., 2019).

Ice stream lateral moraines - Elongated ridges orientated parallel to the former ice flow are observed at the lateral boundaries of Clyde Trough (Fig. 4). They are up to 25 m-high, 1 to 3 km-wide and occur at depths between 50 m and 175 m. These ridges have a steeper trough-proximal slope and are observed on both sides of the trough.

These extensive elongated ridges are interpreted as ice-stream lateral moraines based on their shape, dimensions and location at the margins of the trough (Ottesen et al., 2007; Rydningen et al., 2013; Batchelor and Dowdeswell, 2016; Brouard and Lajeunesse, 2019b). They have been suggested to be formed mainly from the accumulation of subglacial till at the shear zone between fast-flowing ice stream and slow-flowing portions of an ice sheet or ice free terrain (Dyke and Morris, 1988; Stokes and Clark, 1999, 2002; Batchelor and Dowdeswell, 2016).

4.1.3. Proglacial landforms

Two other sets of landforms are identified in the Clyde fjord-cross shelf trough system and characterize the glacial dynamics in front and beyond the receding margin of the ice sheet: iceberg ploughmarks and glaciofluvial fans.

Iceberg ploughmarks - Straight and sinuous V- or U-shaped furrows are observed at varying depths along the fjord-cross-shelf trough system (Figs. 4, 5A and 6A). They are more common on

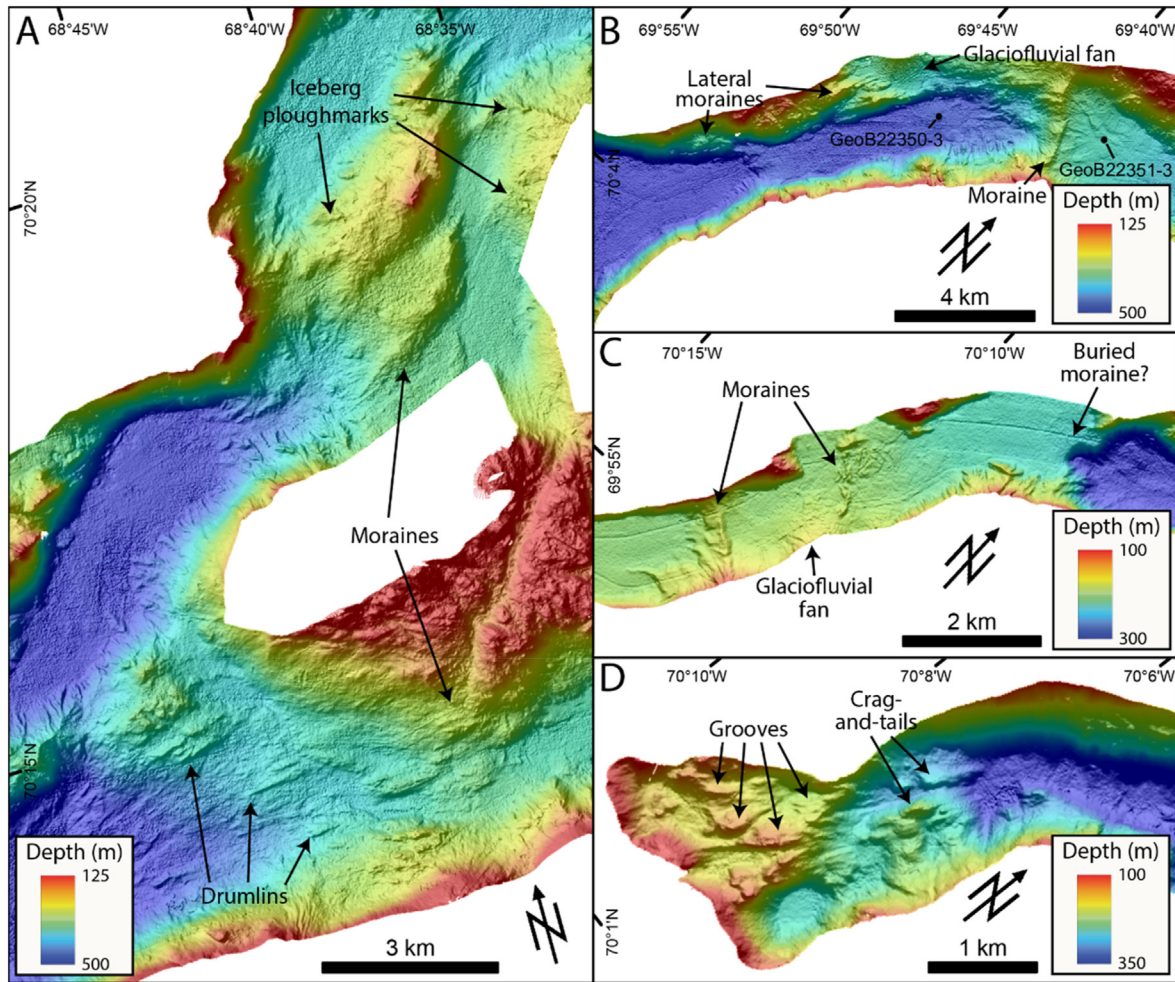


Fig. 6. (A) Multibeam bathymetry of submarine landforms in the outer fjord. (B) Multibeam bathymetry of submarine landforms in the middle fjord. (C) Glaciofluvial fan and moraines in the inner fjord. (D) Crag-and-tails and grooves in Cormack Arm.

the continental shelf, whereas in the fjord they mostly occur on the sill. They are usually associated with berms or levees on either side and often cross-cut each other. They are 2 to 10 m-deep, up to 200 m-wide and in some cases can be traced for >5 km. Two predominant orientations can be distinguished for the larger furrows in the outer trough area: 1) near the shelf break, iceberg ploughmarks superimpose the outermost GZW, are observed at depths ranging between 175 and 225 m and have a NNW to SSE orientation; 2) on the stoss side of the second GZW, ploughmarks are observed at depths between 150 and 200 m and have a nearly orthogonal (SW-NE) along-trough orientation (Fig. 4). Some large zones of chaotic scouring patterns are also identified in the outer trough, regardless of shallower surrounding seafloor area (Fig. 4). They are between 1 and 5 km-wide and present both depressions and mound-like morphologies with irregular furrows. The depressions are generally between 2 and 5 m-deep, while the mounds are <2 m-high. The SE flank of the trough is also densely incised by randomly oriented semi-circular pockmarks (Fig. 2A). They are generally <5 m-deep and rarely exceed 100 m-wide.

Due to their straight and sinuous character, V- and U-shaped cross-profiles and chaotic patterns, these furrows are interpreted as ploughmarks – also termed iceberg scours – from iceberg keels associated with calving outlet glaciers during deglaciation (King, 1976; Vorren et al., 1989; Jakobsson et al., 2011; Dowdeswell et al., 2014; Lewis et al., 2016; Brouard and Lajeunesse, 2019a,

2019b). The SSE oriented ploughmarks suggest influence of the Baffin Island Current (BIC), which delivered large icebergs from northern Baffin Bay in the early phases of deglaciation (Andrews et al., 1998; Jennings et al., 2011), whereas the NE orientated iceberg ploughmarks is probably related to ice calving from the Clyde Ice Stream (CIS) margin. The larger chaotic zones possibly correspond to large iceberg (>5 km²) grounding areas and may have been produced by the ploughing of the seafloor by the keel of larger ice masses that were stuck for long periods of time. Tides and meltwater currents may have caused these iceberg shifts, creating the chaotic pattern. To our knowledge, such features have rarely been identified on continental margins and the genesis presented here remains speculative. The semi-circular pockmarks are interpreted as pits formed by the short-term grounding of icebergs that were semi-buoyant or that turned over, as described by Woodworth-Lynas et al. (1991).

Glaciofluvial fans - Several smooth and gently sloping fan-shaped morphologies are observed on the flanks of the fjord-cross-shelf trough system, at the mouth of tributary valleys (Figs. 5B, 6 B–C). They are generally 1 to 5 km-long and observed at depths between 200 m and 400 m. On their upper reaches, they are dissected by series of parallel 15 m-deep channels. On their lower reaches, they are superimposed by transverse 5 m-high and 200 m to 1 km-wide curvilinear ridges.

These fan-shaped landforms are interpreted as glaciofluvial fans

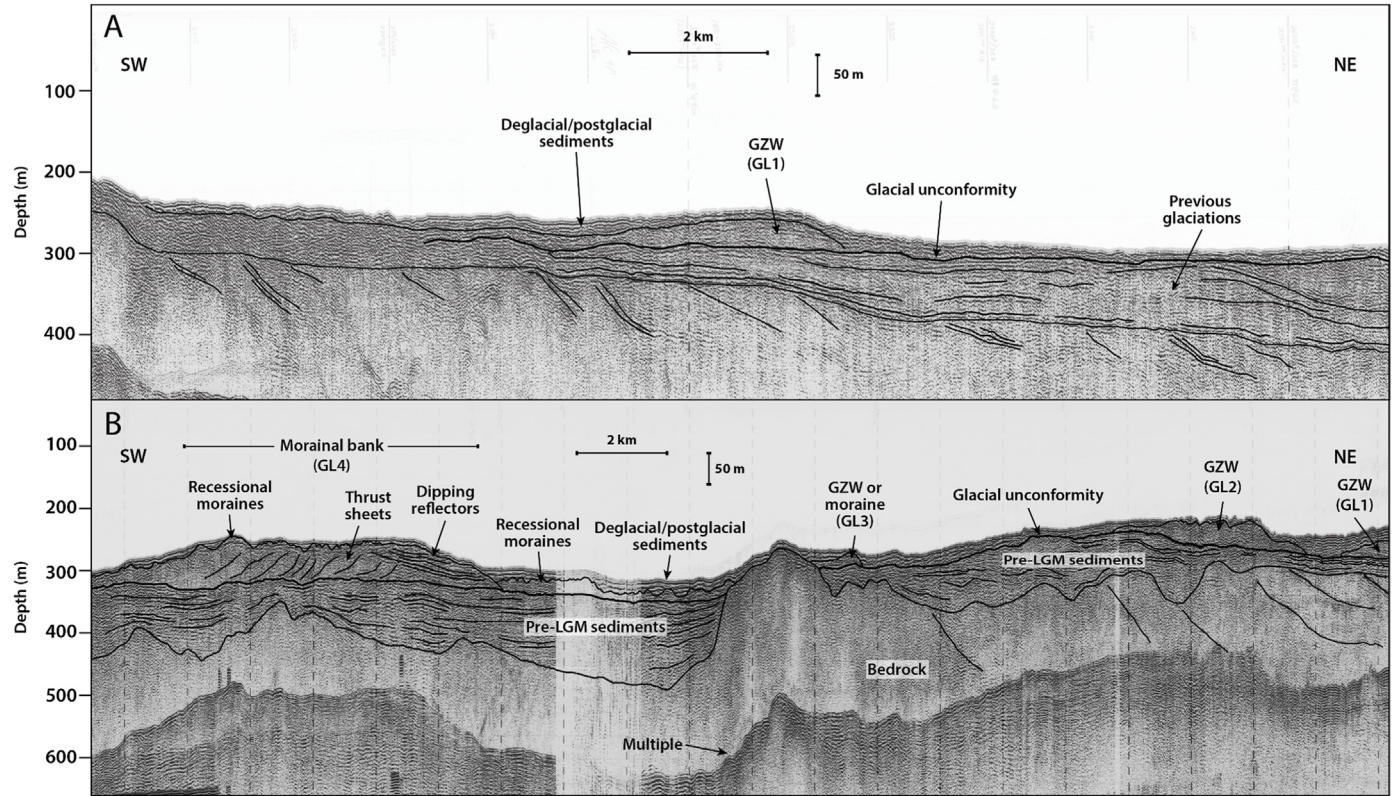


Fig. 7. (A) Airgun profile 78029_AG_275_0130 in the outer Clyde Trough showing GL1 and deeply buried GDFs. (B) Airgun profile 80028_AG_RAYT_257_0200 along Clyde Trough showing the sedimentary assemblages. The depth is based on two-way travel time (TWTT) of 1500 m s⁻¹.

formed by sediment delivery by glacial meltwaters from adjacent alpine valleys (Powell, 1990; Normandeau et al., 2019). Similar landforms were previously identified from several glaciated locations (Powell, 1990; Lønne, 1995; Dowdeswell and Vásquez, 2013; Normandeau et al., 2019; Brouard and Lajeunesse, 2019a, 2019b). Parallel channels are more common on glacially-fed fans suggesting higher turbidity currents activity used for delivering sediments downslope (Dowdeswell and Vásquez, 2013; Batchelor et al., 2018; Normandeau et al., 2019). Transverse curvilinear ridges observed on foreset beds are crescent-shaped bedforms formed by turbidity currents (Normandeau et al., 2019).

4.2. Acoustic stratigraphy

Six acoustic facies (AF) were distinguished from >2500 km of Parasound profiles in the Clyde fjord-cross-shelf trough system. They were differentiated on the basis of their acoustic signatures, bounding reflectors and internal geometries. Additionally, airgun profiles allow identifying the general stratigraphy in the middle to outer trough and in places the limit between the seaward-dipping strata of the bedrock and Quaternary sediments (Fig. 7). They also allow delineating an erosional surface, which represent an unconformity in the sedimentation sequence. This surface is overlain by an acoustically chaotic to semi-transparent unit, which is in turn overlain by a thin unit (<10 m) of high amplitude parallel reflectors. The erosional surface and overlying sediments identified on airgun data likely represent the complete glaciation/deglaciation cycle, with an ice sheet advance across the continental shelf during the LGM followed by deglacial to postglacial sedimentation. The Parasound profiles however allow for a more in-depth analysis of the different facies represented along the system during deglaciation.

4.2.1. AF0: Acoustically impenetrable to homogenous facies

AF0 is an impenetrable and homogenous acoustic facies and forms the acoustic basement in most profiles (Fig. 8A–D). This facies is not visible in some basins where the attenuation of the acoustic signal in thick sediment prevents penetration. It is internally structureless and is characterized by a weak, high-amplitude rugged upper reflector; in most cases it shows an irregular to hyperbolic geometry.

4.2.2. AF1: Acoustically homogenous, non-conformable facies

AF1 rarely exceeds 5 m thickness and is restricted to the outer trough (Fig. 8A). It is characterized by chaotic and discontinuous acoustic reflectors with occasional hyperbolae near the surface. This facies is acoustically homogenous and exhibits weak lower reflectors. It shows in-filled small-scale (~5 m-deep, ~100 m-wide) V-shaped depressions and a non-conformable configuration.

4.2.3. AF2: Acoustically stratified, conformable facies

AF2 is an acoustically stratified and conformable facies with a sharp upper reflector and low to medium amplitude parallel to sub-parallel irregularly-spaced internal reflectors (Fig. 8B–D). AF2 drapes the underlying unit and sometimes exhibits discrete wedge-shape geometries at its lateral boundaries. It is observed over distances of several kilometers in the deeper parts of basins located within the fjord, but is also present at some locations on the inner trough and possibly on the upper slope of the shelf edge (Fig. 7B). AF2 is generally between 5 and 20 m-thick, but reaches >30 m in the inner fjord. This facies is usually observed immediately seaward from grounding line landforms (i.e., GZWs, morainal bank and moraines), although their connection remains elusive.

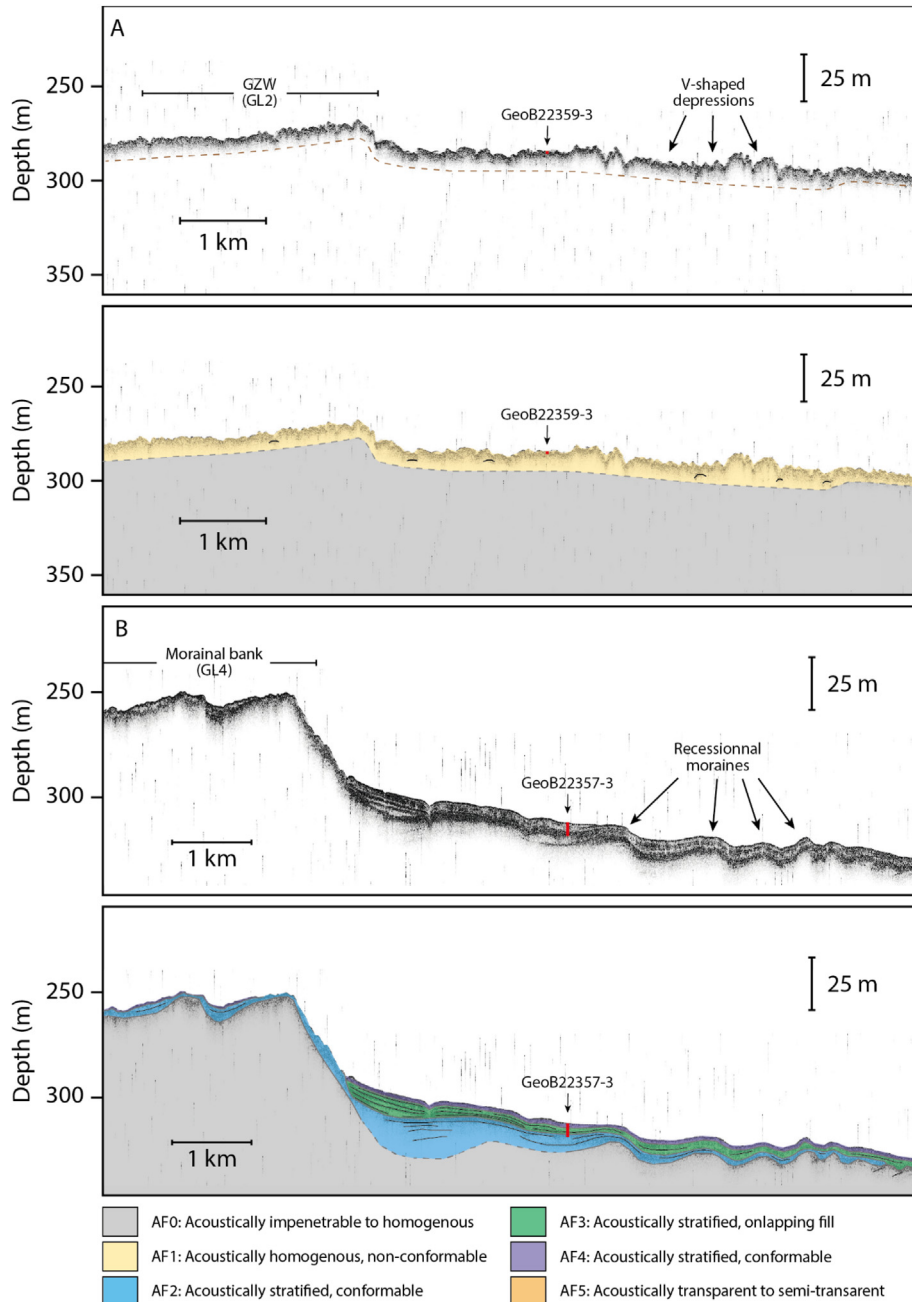


Fig. 8. Parasound profiles along the Clyde Inlet fjord-cross-shelf trough system showing the different acoustic facies (Table 1). See Figs. 2 and 3 for location of the profiles. Color coding for the different acoustic facies is the same as the one used for the lithological facies in Fig. 9.

4.2.4. AF3: Acoustically stratified, onlapping fill facies

AF3 is an acoustically stratified facies with parallel medium to high amplitude reflectors (Fig. 8B–D). It has an onlapping or ponded basin-fill configuration and is interbedded with occasional thicker transparent units. This facies is usually between 10 and 40 m-thick, but can reach >75 m in the fjord. Acoustically chaotic and transparent lenticular sediment bodies are in many cases observed within AF3.

4.2.5. AF4: Acoustically stratified, conformable facies

AF4 is an acoustically stratified facies with parallel, closely spaced high amplitude and opaque reflectors (Fig. 8B–D). It forms a

conformable drape of <5 m on the underlying AF3. It characterizes the uppermost sediment bodies deposited in the Clyde fjord-cross-shelf trough system.

4.2.6. AF5: Acoustically transparent to semi-transparent facies

AF5 is an acoustically transparent to semi-transparent chaotic facies with rare or poorly defined internal reflectors (Fig. 8C–D). Sediment bodies forming AF5 usually have an erosive base, an hummocky surface and are either lenticular or taper on slopes. It is often observed interfingered within the stratified AF2 or AF3. It is generally a few meters-thick, but can exceed 10 m-thick locally. AF5 is mostly observed inside the fjord, near slopes and tributary

valleys.

4.3. Lithological facies

Glacial lithological facies (LF) were identified from the gravity cores collected in the Clyde Inlet fjord-cross-shelf trough system by combining visual core descriptions, photographs of split cores and XRF data. Five facies and three subspecies were determined based on color, texture, sedimentary structures (e.g., lamination, bioturbation) and Ca/Ti ratio changes (Fig. 9). Ratios of calcium (Ca) to titanium (Ti) were used for correlation between the cores along the Clyde Trough transect.

4.3.1. LF1: Unstratified sandy mud with dropstones

LF1 consists of unstratified olive dark gray sandy mud with

dropstones and dispersed pebble-sized clasts. This lithofacies shows no or few traces of bioturbation and occurs in the cores of the outer trough. LF1a consists of a gray coarse sandy mud, IRD-rich facies with occasional sand lenses. LF1b has a more reddish brown color with a finer sandy mud matrix and fewer apparent clast. LF1b is only found in core GeoB22359-3 and is characterized by a high peak in Ca/Ti ratio.

4.3.2. LF2: Poorly sorted diamicton

LF2 only occurs at the base of core GeoB22357-3 and consists of dark gray weakly stratified, poorly sorted muddy-sand matrix diamicton. It is characterized by thick horizons (50–75 cm) of abundant sub-angular to sub-rounded clasts ranging from granules to pebbles, resulting in relatively higher and more chaotic peaks of Ca/Ti ratio. Diamicton beds of LF2 have conformable bedding

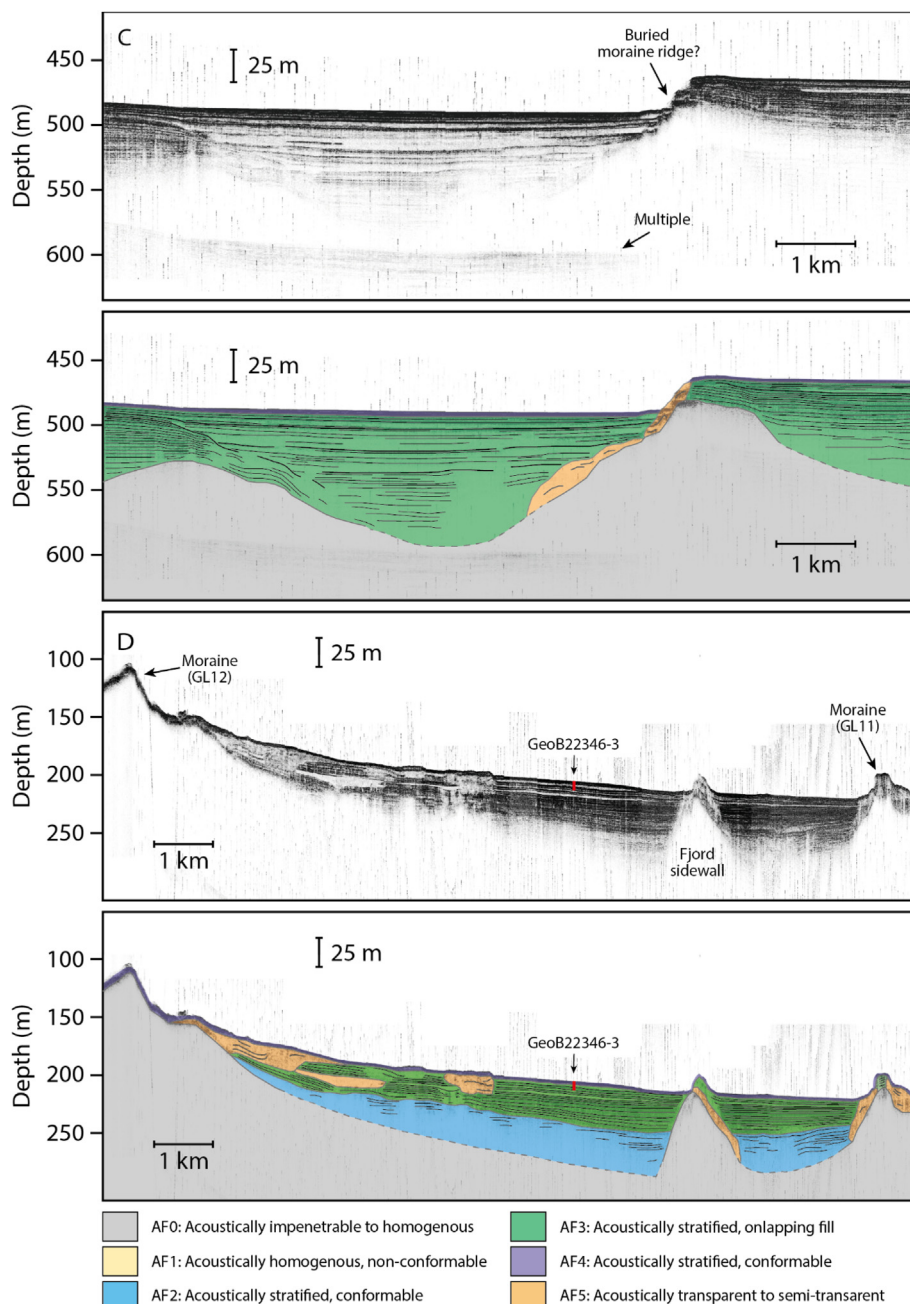


Fig. 8. (continued).

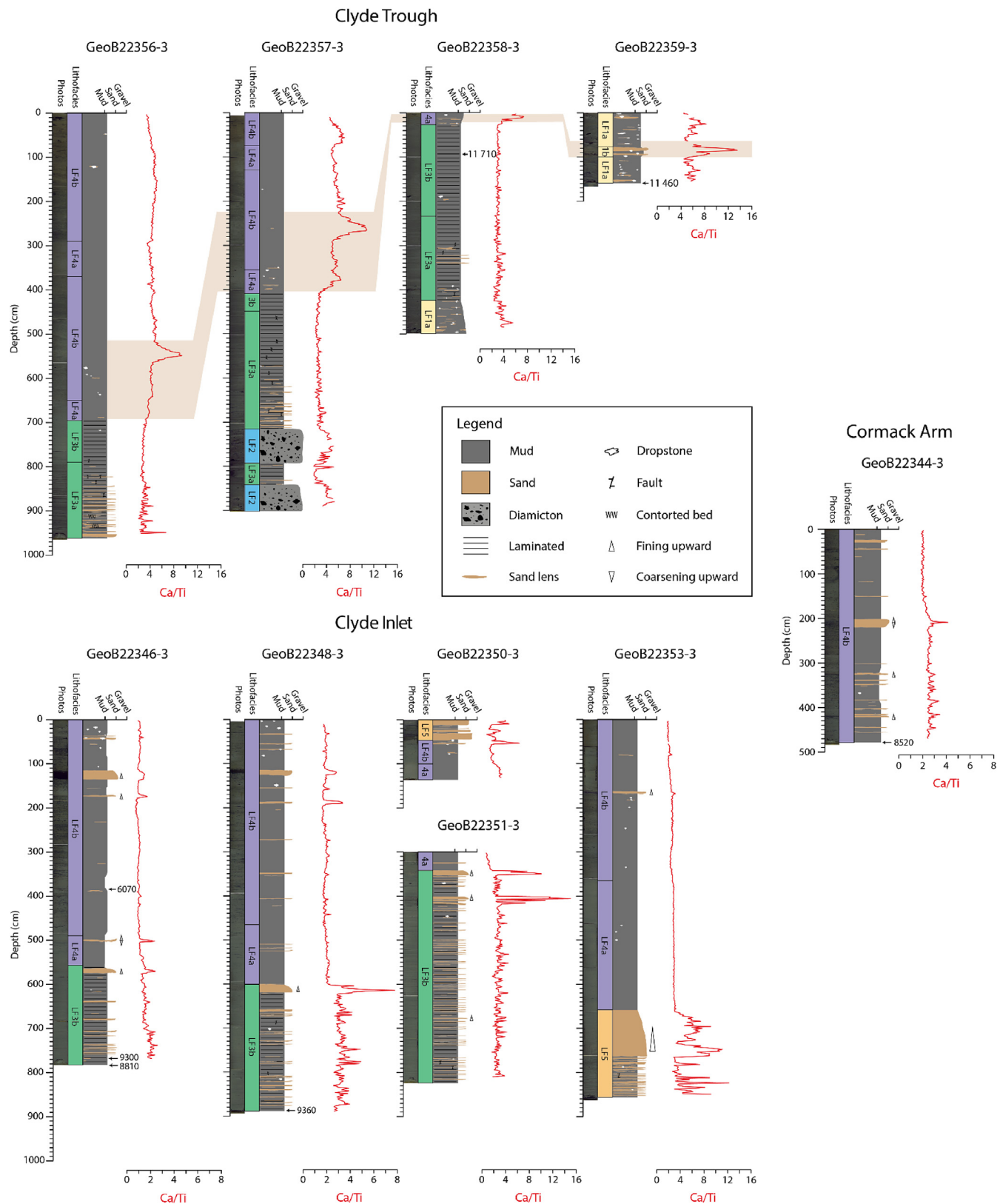


Fig. 9. Simplified lithological logs, Ca/Ti ratios and calibrated radiocarbon ages of sediment cores collected along the Clyde Inlet fjord-cross-shelf trough system. Note that Ca/Ti ratios have a different scale for GeoB22344-3, GeoB22346-3 and GeoB22348-3. Color coding for the different lithological facies is the same as the one used for the acoustic facies in Fig. 8.

contact and are interbedded with massive to laminated and faulted silty mud beds of LF3.

4.3.3. LF3: Laminated mud with sandy layers

LF3 is a laminated gray to dark gray silty mud characterized by a lack of bioturbation and the presence of scattered angular to sub-angular clasts. It also contains individual thin sand laminae that has sharp basal contacts. The sand layers are coarser and thicker at the base of the unit, defining an overall fining upward trend. LF3a is defined by the presence of faulting, as well as more irregular and prominent laminae. LF3b shows no faulting but contains faint thinner beds of coarser sediments. Curves of Ca/Ti ratios from LF3b are chaotic with numerous peaks generally corresponding to coarser laminae. The laminae become less prominent and more spaced upward at the transition from LF3a to LF3b.

4.3.4. LF4: Massive bioturbated silty mud

LF4 consists of massive olive gray, bioturbated silty mud and occurs at the top of most cores, except GeoB22350-3 and GeoB22359-3. This lithofacies generally contains black mottles and few clasts. The transition with the underlying unit is gradational; LF4a is weakly bioturbated, while LF4b contains high concentrations of bioturbation and black mottles. Ca/Ti ratios in the fjord are relatively low with distinct peaks representing sandy layers. In the trough, these ratios are higher and more irregular with peaks representing longer events or of higher magnitude.

4.3.5. LF5: Unstratified sand

LF5 is characterized by unstratified gray coarse sand with lenses of olive gray silty mud and occurs only at the top of core GeoB22350-3 and at the base of core GeoB22353-3. This unit rests on LF4 and shows traces of bioturbation in the silty mud lenses. Ratios of Ca/Ti in LF5 are characterized by chaotic and irregular peaks.

4.4. Correlation of acoustic stratigraphy and lithological facies

Combining the acoustic stratigraphy and lithological facies allows drawing the sedimentary architecture of the Clyde fjord-cross-shelf trough system. Table 2 presents a summary of the acoustic stratigraphy and lithofacies descriptions in their context of unit correlations.

4.4.1. Unit 0: Bedrock or ice-contact sediments

Based on its stratigraphic position, acoustic appearance and rugged upper reflector, Unit 0 represents bedrock and/or ice-contact sediments (Svitski and Shaw, 1995; Streuff et al., 2018). Due to the absence of penetration in coarse sediments, it is usually difficult to differentiate between the two types on acoustic profiles (Streuff et al., 2018; Hogan et al., 2020). Nevertheless, Mesozoic to Tertiary sedimentary bedrock is recognizable on airgun profiles by seaward-dipping strata, whereas ice-contact deposits have a chaotic internal signature (Fig. 7). These profiles also reveal an unconformity that lies above >50 m of undifferentiated Quaternary sediments.

4.4.2. Unit 1: Iceberg-influenced sedimentation

Unit 1, comprising AF1 and LF1, is interpreted as iceberg-influenced sedimentation, with ploughing and subsequent infilling by ice rafted sediments (Woodworth-Lynas et al., 1991; Arosio et al., 2018; Callard et al., 2018; Streuff et al., 2018; Olsen et al., 2022). Hyperbolic signals present in this facies are characteristic of point-source diffractions from dispersed cobbles and boulders (Arosio et al., 2018; Callard et al., 2018). The unstratified structure and high pebble-sized clasts content suggest that iceberg calving

was an important sediment source (Dowdeswell et al., 1994, 2000; Ó Cofaigh and Dowdeswell, 2001; Ó Cofaigh et al., 2013a; Hogan et al., 2016; Sheldon et al., 2016). Its occurrence in heavily iceberg-disturbed area, as shown by multibeam bathymetry (Fig. 4), is consistent with this interpretation. The reddish brown color and the high Ca/Ti ratio of LF1b might correspond to a predominantly detrital carbonate input from northern Baffin Bay – possibly BBDC-0 (Simon et al., 2014; Jackson et al., 2017; Jenner et al., 2018; Lévesque et al., 2020).

4.4.3. Unit 2: Glaciogenic debris-flows

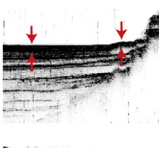
Based on its conformable geometry, stratified acoustic signature and sandy matrix-supported diamicton facies, AF2 and LF2 are interpreted as glaciogenic debris-flows likely sourced during still-stands of the ice margin (Powell, 1990; Powell and Alley, 1997; King et al., 1998; Ó Cofaigh and Dowdeswell, 2001; Flink and Noormets, 2018). The alternating nature of LF2 with the laminated/faulted mud of LF3 is consistent with an origin of distinct pulses of glaciogenic debris-flows interbedded with meltwater plumes (Ó Cofaigh et al., 2013a; Callard et al., 2018; Jenner et al., 2018; Prothro et al., 2018). High sand and gravel content often indicate an ice-proximal sedimentation located within a few kilometers of the grounding line, which requires a stable ice margin over a period of years to decades in case of a thick accumulation (Ó Cofaigh et al., 2008; Dowdeswell et al., 2015; Callard et al., 2018; Prothro et al., 2018). Comparable facies have commonly been identified near glacier-influenced submarine fans and are inferred to be related to the remobilization of glaciogenic debris at the grounding line by abundant subglacial meltwater discharge (Svitski, 1991; King et al., 1998; Ó Cofaigh et al., 2013b; Dowdeswell et al., 2015). The occurrence of such facies at a relatively short distance (<2 km) from former major grounding line positions in the Clyde fjord-cross-shelf trough system therefore support this interpretation.

4.4.4. Unit 3: Ice-proximal glaciomarine sedimentation

Unit 3, comprising AF3 and LF3, is interpreted as stratified ice-proximal glaciomarine sedimentation (Ó Cofaigh and Dowdeswell, 2001; Hodgson et al., 2014; Brouard and Lajeunesse, 2019a; Trottier et al., 2020; Olsen et al., 2022). The well-preserved laminations suggest fallout sediment deposition from meltwater plumes (Svitski, 1991; Ó Cofaigh and Dowdeswell, 2001; Sheldon et al., 2016; Jenner et al., 2018; Callard et al., 2020; Olsen et al., 2022). Laminae probably correspond to seasonal changes in sedimentation, where finer layers result from reduced subglacial meltwater input during winter (Flink and Noormets, 2018; Prothro et al., 2018). The sand layers with sharp basal contacts correspond to deposition by turbidity currents or turbid meltwaters sourced from the ice margin (Sheldon et al., 2016; Olsen et al., 2020). Dispersed clasts, indifferentially found in fine or coarse laminae are interpreted as ice-raftered debris (IRD). The occurrence of randomly dispersed IRDs indicates that rain-out from icebergs was a minor sedimentation process contributing to LF3 (Svitski, 1991; Sheldon et al., 2016) and/or accumulation rates were high, with dilution of the IRD signal (Svitski and Shaw, 1995; Dowdeswell et al., 2000; Olsen et al., 2022). The latter interpretation is in agreement with the lack of bioturbation (Ó Cofaigh and Dowdeswell, 2001; Sheldon et al., 2016; Callard et al., 2020). Rapid sediment loading causing minor submarine slope failures may explain the abundant occurrence of faults in LF3a (Callard et al., 2018; Allaart et al., 2020). The decrease of the thickness and grain size of the laminae and the disappearance of faulting in LF3b together reflect a progressively distant marine terminating ice margin, representing ice-proximal to distal glaciomarine sedimentation (Ó Cofaigh and Dowdeswell, 2001; Dowdeswell et al., 2015; Streuff et al., 2017; Callard et al., 2018, 2020; Jenner et al.,

Table 2

Description of sedimentary units identified in the sub-bottom profiles data and sediment cores from the Clyde fjord-cross-shelf trough system.

Unit	Acoustic facies	Description	Lithological facies	Example	Description	Interpretation
U0	AF0	Acoustically impenetrable. Homogenous and structureless. High-amplitude upper reflector. Occasional hyperbolas.				Acoustic basement (bedrock/ice-contact)
U1	AF1	Semi-transparent and chaotic. Discontinuous and homogenous reflectors. Non conformable geometry.	LF1		Unstratified olive dark gray sandy mud. Randomly disseminated pebble-sized clasts. Few traces of bioturbation.	Iceberg-influenced sedimentation
U2	AF2	Acoustically stratified. Low to medium amplitude parallel to sub-parallel internal reflectors. Conformable geometry.	LF2		Dark gray muddy-sand matrix diamicton. Weakly stratified and poorly sorted. Dispersed flows sub-angular to sub-rounded clasts. Interbedded with LF3.	Glacial debris
U3	AF3	Acoustically stratified. Medium to high amplitude parallel internal reflectors. Basin fill (ponded) or onlapping geometry.	LF3		Laminated gray to dark gray silty mud. Sand laminae with sharp basal contact. Lack of bioturbation. Occasional clasts. Presence of faults at the base.	Ice-proximal glaciomarine sedimentation
U4	AF4	Acoustically stratified. High amplitude parallel and closely-spaced opaque reflectors. Conformable geometry.	LF4		Massive olive gray silty mud. Moderately to heavily bioturbated. Presence of black mottles and rare clasts. Gradational transition from LF3.	Ice-distal hemipelagic sedimentation
U5	AF5	Acoustically transparent to semi-transparent. Chaotic with rare internal reflectors. Hummocky surface and lenticular shaped geometry.	LF5		Unstratified gray coarse sand with bioturbated lenses of olive gray silty mud.	Turbidites and mass-movement deposits

2018; Allaart et al., 2020).

4.4.5. Unit 4: Ice-distal hemipelagic sedimentation

The acoustic appearance of AF4 and LF4 corresponds to typical ice-distal hemipelagic sedimentary systems. Comparable acoustic facies have been identified in polar regions and are usually deposited by meltwater run off, tidal processes and, in a lesser extent, ice rafting sedimentation (Svitski, 1991; Svitski and Shaw, 1995; Hogan et al., 2016, 2020; Callard et al., 2018; Arosio et al., 2018; Streuff et al., 2018). The sediments show little to no IRDs, suggesting a distal or terrestrial ice margins (Svitski, 1991; Svitski and Shaw, 1995; Sheldon et al., 2016; Callard et al., 2018; Olsen et al., 2020, 2022; Svitski et al., 2022). The transition from weakly (LF4a) to intensively (LF4b) bioturbated mud essentially represents decreasing sedimentation rates with landward retreating glacier fronts (Callard et al., 2018; Jenner et al., 2018). The heavy bioturbation indicates hemipelagic sedimentation, similar to that of today.

4.4.6. Unit 5: Turbidites or mass-movement deposits

Based on the transparent acoustic signature of AF5 and the unstratified sandy structure of LF5, unit 5 is interpreted as a coarse-grained unit from various high-energy sources such as turbidites or mass-movement deposits, which is supported by its occurrence at the foot of slopes or in front of glacially-fed tributary valleys (Svitski and Shaw, 1995; Streuff et al., 2017; Hogan et al., 2020; Olsen et al., 2022). The presence of bioturbated mud lenses in between beds of coarse sand suggest that Unit 5 is not the continuity

of Unit 4, but they are rather intermittent. The position of the coring sites in front of major valley deltas may indicate distinct cohesionless mass-movement deposits from remobilized coastal sediments (Gilbert et al., 1990).

4.5. Radiochronology

Seven ages were obtained from radiocarbon dated material collected from the sediments cores (Table 3).

In Clyde Trough, at the base of core GeoB22359-3, mixed benthic foraminifera in iceberg-influenced sediments (LF1) provided an age of 11.5 ka cal. BP. A shell fragment from ice-proximal glaciomarine sediments (LF3), at 92 cm from the top of core GeoB22358-3, yielded an age of 11.7 ka cal. BP. These ages in deglacial sediments provide a minimum age for the deglaciation of the outer trough (Fig. 2). However, the age in GeoB22358-3 shows that it is most likely an underestimation of the deglaciation as the sample was collected near the top of the core.

In the inner Clyde Inlet (Fig. 3), three ages were provided from samples collected in ice-proximal glaciomarine sediments (LF3) from the base of two sediment cores. The sample at the base of sediment core GeoB22348-3, taken approximately 25 km from the fjord head, revealed an age of 9.4 ka cal. BP. The base of sediment core GeoB22346-3, taken 10 km from the fjord head, yields an age of 8.8 ka cal. BP. A shell fragment near the base of GeoB22346-3, yielding an age of 9.3 ka cal. Ka BP, was rejected because it was inconsistently older than the benthic foraminifera sample taken a few centimeters below. The shell fragments could have been

Table 3

Radiocarbon and calibrated radiocarbon ages from material collected in sediment cores.

Core number	Depth in core (cm)	Dated material	Laboratory ID	^{14}C age yr BP	Calibrated age yr BP (2σ)
GeoB22344-3	472–483	Mixed benthic foraminifera	AWI-2620.1.1	8280 ± 90	8520 (8280–8840)
GeoB22346-3	387	Shell fragment	AWI-1726.1.1	5930 ± 50	6070 (5900–6250)
GeoB22346-3	765	Shell fragment	AWI-1727.1.1	8900 ± 190	9300 (8770–9850)
GeoB22346-3	766–783	Mixed benthic foraminifera	AWI-2619.1.1	8510 ± 100	8810 (8500–9120)
GeoB22348-3	888–896	Mixed benthic foraminifera	AWI-2618.1.1	8940 ± 100	9360 (9050–9600)
GeoB22358-3	92	Shell fragment	AWI-1728.1.1	$10,670 \pm 177$	11,710 (11,190–12290)
GeoB22359-3	156–166	Mixed benthic foraminifera	AWI-2617.1.1	$10,500 \pm 100$	11,460 (11,170–11800)

The AMS ^{14}C ages were calibrated within the age-depth modelling process, using the online software Calib 8.2 with the Marine20 radiocarbon age calibration curve (Heaton et al., 2020). A local reservoir correction (ΔR) of 81 ± 18 was used to account for the regional offset of the world ocean ^{14}C age, as determined by Piękowska et al., 2022).

reworked, as the age range is consistent with a reworked shell found in a delta at the fjord head and another one found in a nearby tributary valley (Briner et al., 2007). Therefore, the benthic foraminifera sample is favored as being the most reliable age available for the base of that core. An age of 6.1 ka cal. BP was also obtained from a shell fragment at 387 cm downcore, in ice-distal glaciomarine sediments (LF4).

Similarly, a foraminifera sample collected in ice-distal glaciomarine sediments (LF4) from the base of sediment core GeoB22344-3 yielded an age of 8.5 ka cal. BP. It thus provides a minimum age for full deglaciation of Cormack Arm.

5. Discussion

5.1. Extent and retreat of the LIS margin

The analysis of the multibeam bathymetry, acoustic profiles and lithological facies allowed the identification of landforms and sedimentary assemblages that are typical of high-latitude fjord-cross-shelf trough systems (e.g., Praeg et al., 2007; Winsborrow et al., 2010; Ó Cofaigh et al., 2013b; Sheldon et al., 2016; Slabon et al., 2016; Brouard and Lajeunesse, 2017; Ottesen et al., 2022). They provide valuable information on the maximal extent of the LIS margin and its retreat patterns along the entire Clyde fjord-cross-shelf trough system. However, deglacial ages on the shelf and nearby fjords of Baffin Island are scarce and correlations with other systems is therefore tentative. The radiocarbon dated horizons of the cores are stratigraphically too shallow to construct reliable age extrapolations to the base of the deglacial units. Nevertheless, they represent minimum-limiting ages at the coring sites and thus provide some constraints on ages of the deglaciation patterns we present. The compatibility with land-based studies provides independent corroboration that allow us to draw a more accurate chronology of the deglaciation for the Clyde fjord-cross-shelf trough system (Fig. 10).

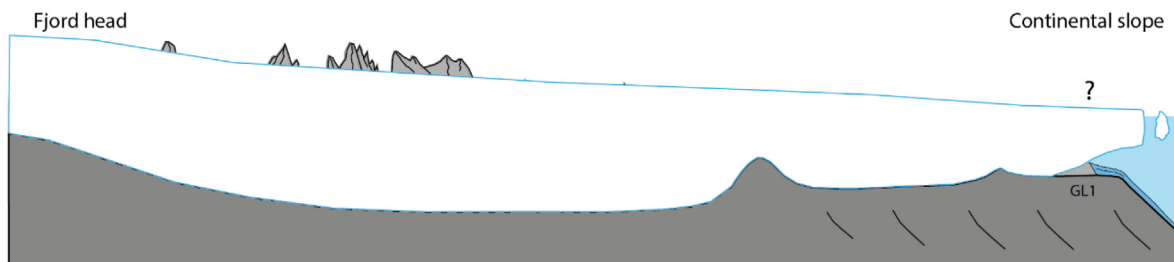
5.1.1. LGM extent and collapse of the clyde ice shelf

Couette et al. (2022) asserted that the LIS did not reach the shelf break in Clyde Trough on the basis of geomorphological, sedimentological and glaciological evidence. They argued that the absence of gullies on the trough mouth fan and glacial lineations in the outer trough – which are both diagnostic of a grounded ice margin extending at the shelf break – suggest that the LIS had a receded position in Clyde Trough. It is however possible that the extensive iceberg ploughmarks observed in the outer trough have obscured any landforms that provide evidence for the LIS margin reaching the shelf break during the LGM. In the absence of such evidence, the GZWs observed near the shelf edge are therefore identified as the most probable maximal position of the LIS in Clyde Trough during the LGM (Fig. 10a). The onset of deglaciation around Baffin Bay appears to have occurred between 16 and 14.6 ka cal. BP

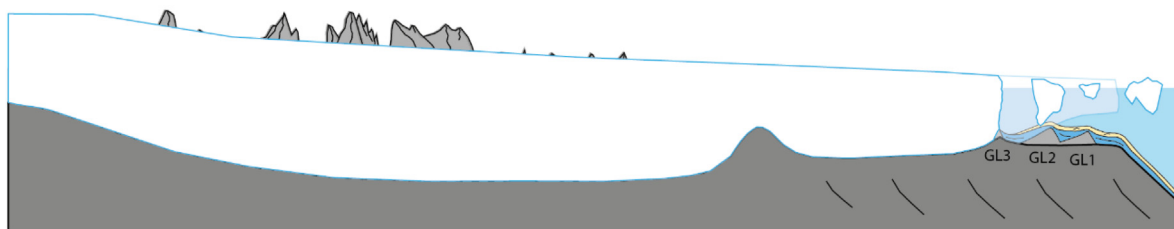
on eastern Baffin Island (Jennings, 1993; Briner et al., 2007; Margreth et al., 2017) and western Greenland (Sheldon et al., 2016; Jennings et al., 2017). This timing for the deglaciation of the shelves is in agreement with cosmogenic exposure dating from the Clyde Foreland, where deglaciation is interpreted to have started at ~15 ka BP (Briner et al., 2005). As no direct dating has yet yielded absolute ages on these landforms, it can not be asserted with certitude which of the two GZWs, if any, represent the LGM maximal extent. The change in orientation and density of iceberg ploughmarks suggest that the CIS margin was possibly grounded at GL2 during the early phases of deglaciation, when numerous icebergs were released into Baffin Bay and transported via the Baffin Island Current (Andrews et al., 1998). The large iceberg ploughmarks parallel to the trough on the stoss side of GL2 and the IRD-rich facies in the outer trough are, in turn, evidence of a period of extensive iceberg release provoked by the collapse of the Clyde ice shelf and rapid retreat of the CIS (Fig. 10b). Therefore, this period of rapid ice decay might correspond to Meltwater Pulse 1a (MWP-1a – 14.6–14.0 ka cal. BP; Carlson, 2009; Harrison et al., 2018; Lin et al., 2021), which coincides with the release of icebergs and detrital carbonate-rich sediments into Baffin Bay (BBDC layer 1–~14.2–13.7 ka cal. BP) from northwestern Greenland and the eastern CAA (Andrews et al., 1998; Simon et al., 2012, 2014; Jackson et al., 2017).

It is unclear why the LIS margin did not reach the shelf break in Clyde Trough, as ice extended across the continental shelf in Lancaster Sound as well as in the Buchan and Scott trough systems of northeastern Baffin Island (Li et al., 2011; Brouard and Lajeunesse, 2017). Recent studies (i.e., Miller et al., 2002; Margreth et al., 2017) also suggest that the ice margin did not reach the shelf break on Cumberland Peninsula (eastern Baffin Island). The position of the ice margin at the LGM along the coast of eastern Baffin Island was most probably variable. Clyde Trough might represent a zone of transition between the “Big ice” model of northeastern Baffin Island and the “Just-Right ice” model observed on Cumberland Peninsula (see Miller et al., 2002). This intermediate position was also reported in Sam Ford Trough – just north of Clyde Trough –, although this system is considered to have been occupied by slow flowing ice during the LGM (Brouard and Lajeunesse, 2017). Slower flowing ice could also explain the receded position of the ice margin in Clyde Trough, as sparse and undefined glacial lineations in the outer trough suggests limited ice streaming activity at the LGM. However, the lack of glacial lineations on the outer trough possibly reflects the significant disturbance of the seafloor by iceberg ploughmarks. Nonetheless, it is worth noting that a slow ice flow regime was observed for the adjacent Clyde Lowlands, where ice flowing through Ayr Lake was non-erosive and slow flowing in its outermost part (Briner et al., 2005). The opening/diffluent configuration of the outer trough could have favored reduced ice velocity, thus limiting the formation of glacial lineations at the base of the ice stream. A reduced ice velocity could result from a limited catchment size due to the presence of more competent ice stream

a) Last Glacial Maximum (ca. 24 000 BP) - Full-glacial conditions

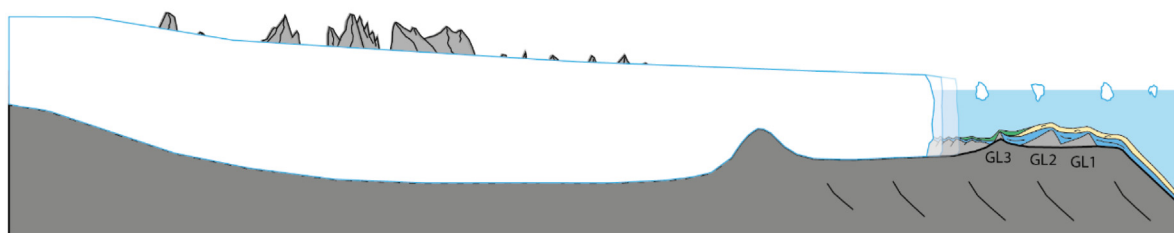


b) Early deglaciation (ca. 14 600 BP) - Ice shelf collapse

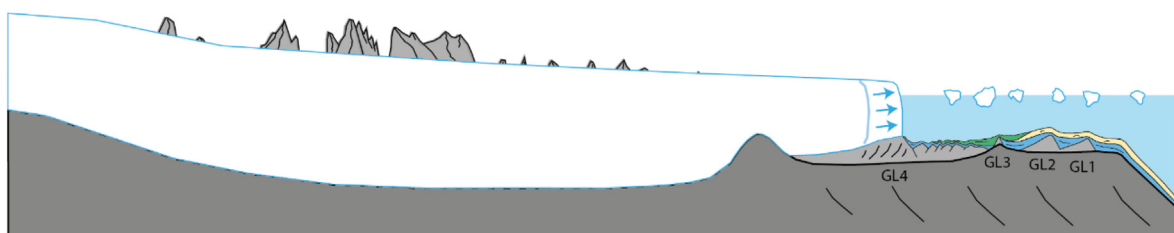


c) Late glacial (ca. 14 600-11 700 BP) - Deglacial stillstands and readvances

i) Recessional moraines



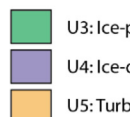
ii) Morainal bank



U0: Bedrock/ice-contact deposits

U1: Iceberg-influenced sedimentation

U2: Glacial debris-flows



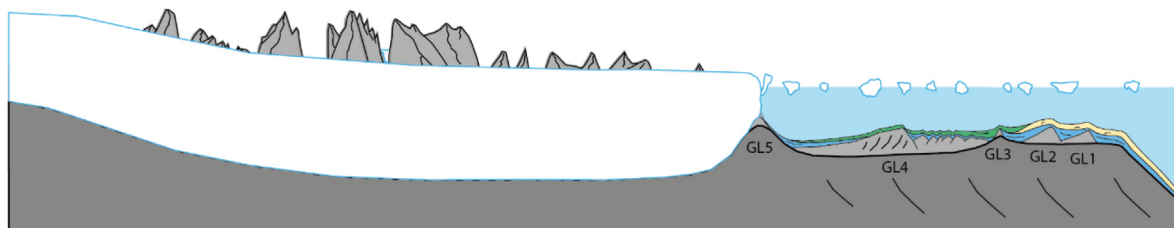
U3: Ice-proximal glaciomarine sedimentation

U4: Ice-distal hemipelagic sedimentation

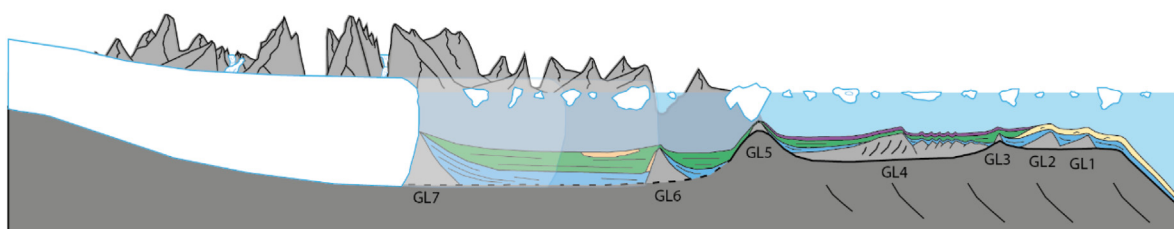
U5: Turbidites and mass-movement deposits

Fig. 10. Schematic representation of the ice dynamics on the shelf corresponding to the different stages of ice retreat during deglaciation in Clyde fjord-cross-shelf trough system.

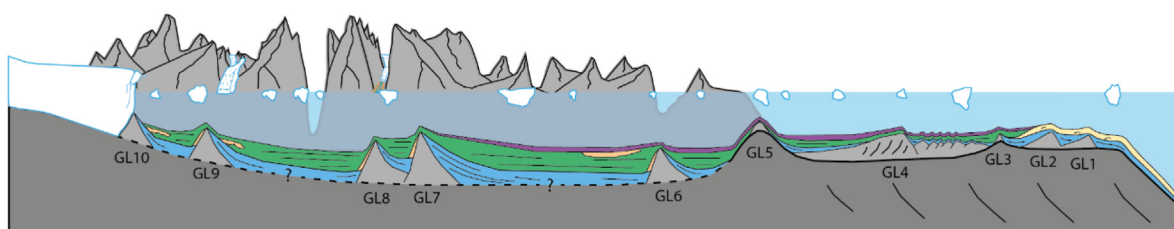
d) End of Younger Dryas (11 700 BP) - Fjord mouth sill stillstand



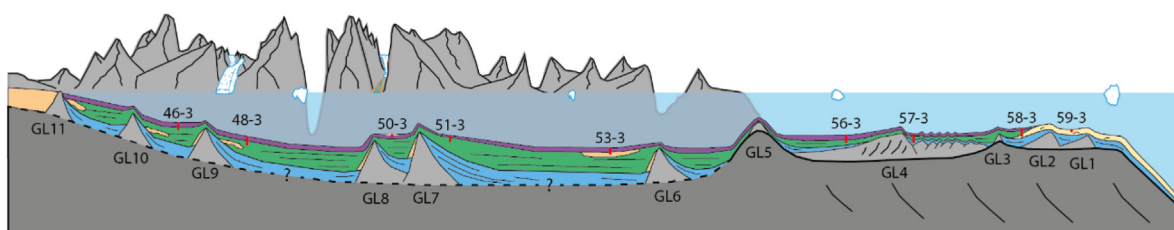
e) Early Holocene (11 700-9500 BP) - Fast retreat into the fjord



f) Cockburn substage (9500-8000 BP) - Fjord head stillstands or readvances



g) Late Holocene (8000 BP - Now) - Paraglacial conditions



- | | |
|--------------------------------------|---|
| U0: Bedrock/ice-contact deposits | U3: Ice-proximal glaciomarine sedimentation |
| U1: Iceberg-influenced sedimentation | U4: Ice-distal hemipelagic sedimentation |
| U2: Glacial debris-flows | U5: Turbidites and mass-movement deposits |

Fig. 10. (continued).

system on either side of the Clyde fjord-cross-shelf trough system. Similar observations have been made on the shelf of northeastern Baffin Island, where piracy of ice drainage basins controlled the volume of ice flow into Sam Ford Trough system (Brouard and Lajeunesse, 2019c). Additionally, the CIS was sustained by cold-based ice on the banks in front of the Clyde and Aston lowlands (Briner et al., 2005). GZWs geometry indicates that cold-based ice also had a receded position on the inter-trough on both sides of Clyde Trough. Sediment assemblages on the Baffin slope further support that position, at least for the later part of the LGM (Jenner et al., 2018). Stacked tills underneath GL1 indicate that some earlier glaciations were, however, more extensive, as previously proposed by various authors for Arctic Canada (i.e., Miller et al., 1977; Evans and Rea, 1999).

5.1.2. Slow late glacial retreat on the shelf

The absence of large GZWs in the middle and inner trough suggests that the ice-retreat following the initial breakup of the CIS occurred in a steady fashion as shown by sets of recessional moraines (Fig. 10c i). This slow retreat pattern differs from observations from other trough systems of northeastern Baffin Island, where deglaciation occurred in a more stepwise pattern with prolonged stillstands indicated by GZWs (Brouard and Lajeunesse, 2017). This deglaciation pattern, situated on the retrograde sloping part of Clyde Trough, is uncommon compared to other global occurrences which generally present few stillstand indicators and are usually attributed to a rapid ice margin retreat (Weertman, 1974; Favier et al., 2014; Wise et al., 2017). Similar variations in style and rate of ice retreat along a continental shelf has also been observed on the Antarctic Peninsula (Dowdeswell et al., 2008; Ó Cofaigh et al., 2014 and references therein) and may thus reflect the influence of local controls (i.e., bathymetry and topography) on ice dynamics of northeastern Baffin Island (see section 5.2).

The morainal bank (GL4) in the middle trough indicates a stage of ice margin readvance and short-term stabilization during the generally slow deglaciation of the trough (Fig. 10c ii). It aligns roughly with lateral moraines dated by Briner et al. (2005) near Patricia Bay, indicating that this event occurred at $\sim 12.5 \pm 0.7$ ka. It is therefore probable that an ice margin readvance during the colder Younger Dryas (~ 12.9 – 11.7 ka BP) favored the formation of the morainal bank. Regardless of their genesis as glaciectonic push-and-thrust or crevasse-squeezed ridges, the transverse and zigzag-shaped ridges on the morainal bank suggest readvance of the LIS margin. These landforms may reflect warm-based fast flow conditions changing to cold-based freeze-on conditions near the ice margin (Clark et al., 2003; Laberg et al., 2009). Cold-based conditions at the ice-margin can be caused by ice thinning, fast downward advection of cold surface ice or basal freezing of the ice stream termination (Clark et al., 2003). Zigzag-shaped ridges have also been associated to ice readvances on the Værøy and Røst morainal banks, in northern Norway (Laberg et al., 2009). The Røst morainal bank is also seismically similar to the middle trough morainal bank with its folded reflectors at the front and the irregular thrusted sheets in its core (Laberg et al., 2009). Folding and thrusting of sediment sheets by glaciectonism (Fig. 7B), which is caused by movements at the front of the glacier (i.e., a readvance of the LIS margin), have been speculated to increase the height of ice-contact deposits (Powell, 1990; Lønne, 1995; Lyså and Vorren, 1997).

The moraine system on top of a bedrock sill at the fjord mouth (GL5) indicates that the ice margin stabilized there for a short period (Fig. 10d). In the cores collected along Clyde Trough, ages of 11.7 and 11.5 ka cal. BP below the transition from ice-proximal glaciomarine sediments to ice-distal hemipelagic sediments

provide a minimal age for the ice margin retreat into the fjord. This transition is also marked by a peak in Ca/Ti in the shelf cores, corresponding to an increase in detrital carbonate-rich sediments (BBDC layers) from northern Baffin Bay. This increase was also recorded along West Greenland and the onset of this event was dated at ~ 11.6 ka cal. BP (Jennings et al., 2014, 2017). This timing for ice retreat from the fjord-mouth at the onset of the Holocene is further supported by data from Scott Trough suggesting ice-distal sedimentation from ~ 12 ka cal. BP (Osterman and Nelson, 1989). Cosmogenic exposure dating from the continental domain indicates that the LIS margin was located at the Clyde Inlet mouth until $\sim 11.7 \pm 2.2$ ka (Briner et al., 2005). These results suggest that the ice margin retreated into Clyde Inlet from the bedrock sill at the end of the Younger Dryas. Stabilizations commonly occur at fjord mouths due to the narrowing of the ice stream width, which reduces the ice flux across the grounding line (Åkesson et al., 2018). This stabilization could also be the result of a forced equilibrium in glacial mass balance, where accumulation is too high for the ice sheet margin to retreat into the deeper and narrower fjord but ablation is too high to allow a readvance onto the shelf and the open sea (Syvitski and Shaw, 1995).

5.1.3. Episodic early holocene retreat in the fjord

The multibeam bathymetry imagery and acoustic sub-bottom profiles show series of moraine systems along the fjord, indicating a step-wise retreat of the LIS margin in the early Holocene, punctuated by intervening periods of fast retreat (Fig. 10e). Two continental moraine ridges located 10 km and 25 km up-fjord from Ailsa Island yielded cosmogenic exposure ages of 11.2 ± 1.2 and 10.0 ± 1.5 ka, respectively (Briner et al., 2007). These ages represent minimum ages for the deglaciation and are probably coeval or younger than the outer fjord moraine (GL6).

Few ages are available in the middle section of Clyde Inlet. However, basal ages collected in three lakes near the adjacent Inugsuin Fjord constrain the deglaciation of the middle section to ~ 10.5 ka cal. BP (Thomas et al., 2010). Ice retreat was probably more or less synchronous in Clyde Inlet, as the continental moraine ridges in the outer fjord yield slightly older ages and a bedrock sample from an unnamed island yielded a cosmogenic exposure age of 10.2 ± 2.2 ka (Briner et al., 2007). Furthermore, cosmogenic dating in Naqsaq Valley indicate alpine glacier stabilization and moraine deposition at $\sim 10.2 \pm 0.2$ ka (Young et al., 2021). It is therefore possible that the middle fjord moraines (GL7 and GL8) were deposited around that time.

During the Cockburn substage, multiple moraines were deposited in the inner fjord and at the fjord head (Fig. 10f). Wood and shell samples collected in a tributary valley 40 km upstream from the fjord head by Briner et al. (2007) yielded identical ages of ~ 9.3 ka cal. BP for deglaciation of the inner fjord. These ages are in agreement with new basal ages from sediment cores GeoB22348-3 and GeoB22346-3 (Fig. 9), which in turn are constraining the timing of the inner fjord moraines (GL9–GL11) between 9.4 and 8.8 ka cal. BP. Similarly, radiocarbon ages from shells collected in deltas at the head of Clyde Inlet indicate that the ice margin retreated beyond the fjord head between 9.1 and 8.6 ka cal. BP (Briner et al., 2007). Similar ages from adjacent Inugsuin Fjord and Sam Ford Fjord corroborate these observations (Andrews and Drapier, 1967; Briner et al., 2009a; Syvitski et al., 2022). An ice-contact delta located at the fjord head yielded cosmogenic exposure age of ~ 8.3 ka ± 0.3 ka (Briner et al., 2007; Young et al., 2013). Radiocarbon ages collected 4 km upstream of the ice-contact delta yielded an age of ~ 7.9 ka cal. BP for the deglaciation of the fjord head (Briner et al., 2007). Deglaciation of the fjord head is marked by a steep decline in Ca/Ti, corresponding to a decrease in coarser sediment input from the ice margin directly into the fjord. The age of ~ 7.9 ka cal. BP is also in

agreement with the shell sample from core GeoB22346-3 indicating that ice had retreated from the fjord head before 6.2 ka cal. BP.

The results from Clyde Inlet notably contrast with models previously proposed from eastern Baffin Island, where the LIS was believed to have retreated in a catastrophic pattern along the fjords (Briner et al., 2007, 2009a). Alternatively, the results support a more episodic deglaciation model with multiple ice margin stabilizations and moraine formation proposed for fjords of northeastern Baffin Islands (Brouard and Lajeunesse, 2019a).

Subsequently to the withdrawal of its ice margin from Clyde Inlet (Fig. 10g), the LIS began a slow retreat towards the south until the Barnes Ice Cap became isolated (Miller et al., 2005; Briner et al., 2009b). The LIS and local glaciers receded beyond their current position until the onset of the Neoglacial ~4.5 ka BP (Miller et al., 2005; Young et al., 2015). During that period, cooler climatic conditions prevailed and local glaciers readvanced into the fjord, as marked by lateral moraines from tributary valleys and glaciofluvial fans (Fig. 6A–B). Rapidly deposited layers are identified in cores of the inner fjord and are marked by sharp peaks in Ca/Ti ratios that could relate to these readvances. These coarse layers could also either represent increased sediment input by glacial meltwater or deposits by glacier-lake outburst floods caused by the oscillation of the Barnes Ice Cap repeatedly blocking the Clyde River outlet (Barnett and Holdsworth, 1974; Andrews and Barnett, 1979).

5.2. Controls on stabilizations and variability of ice retreat

Several external (e.g., atmospheric temperatures, changes in sea level and ocean-driven melting) and local factors (e.g., topography and bathymetry) have possibly asserted a certain control on the deglaciation patterns in the Clyde fjord-cross-shelf trough system. Comparing the chronology presented in the previous section to a compilation of climatic records allows establishing correlations between the deglaciation and potential factors that may have influenced retreat of the ice margin across the system (Fig. 11).

5.2.1. External forcing as the principal driver of ice retreat patterns

The temporal framework presented in the previous section suggest that climate played a dominant role in driving first-order deglaciation patterns in Clyde Inlet, as ice retreat coincides with periods of warming climate and stabilizations are synchronous with cooling events (Fig. 11). In turn, sea level changes and oceanic forcing might also have influenced the retreat rates of the ice margin along the Clyde fjord-cross-shelf trough system (Fig. 11).

Rapidly rising sea-level (>40 mm/year; Lambeck et al., 2014) probably favored the initial collapse of the Clyde ice shelf and rapid retreat of the CIS in the early phases of the deglaciation (Couette et al., 2022). Changes in the eustatic level may have provoked the lift-off of the local ice shelf, increasing the area of the ice margin in contact with the water column, making it more vulnerable to ocean forcings (Joughin et al., 2012; Jamieson et al., 2014; Jennings et al., 2018). The global sea-level rise initiated at ~16.5 ka eventually led to the ice front destabilization, which induced rapid retreat of the ice margin (~25 m/year). Rapidly rising global sea level has been speculated to have triggered the collapse and/or rapid retreat of marine-based ice sheets in the Northern Hemisphere following the LGM (e.g., Winsborrow et al., 2010; Jakobsson et al., 2011; Rydningen et al., 2013; Hogan et al., 2016; Arndt et al., 2017; Callard et al., 2018). In turn, the timing of ice-margin retreat from outer Clyde Trough is synchronous with the onset of the Bølling–Allerød interstadial (~14.5–12.9 ka BP), a period of globally warmer temperatures (Rasmussen et al., 2014). It also coincides with extensive ice mass loss around Baffin Bay, as ice streams were retreating from the outer shelf in Western Greenland (i.e., Sheldon et al., 2016;

Jennings et al., 2017) and large numbers of icebergs were released from northern Baffin Bay (i.e., Andrews et al., 1998; Simon et al., 2012; Jackson et al., 2017). Reduced global sea level rise during the second half of the Bølling–Allerød (~12 mm/year – Lambeck et al., 2014) probably contributed to a slow-down of the ice-margin retreat in Clyde Trough (~12.5 m/year). However, lower rates of sea level rise alone do not explain the slower deglaciation pattern, as it was not observed in neighbouring troughs (Brouard and Lajeunesse, 2017).

The beginning of the Younger Dryas (~12.9–11.7 ka BP) was regionally marked by an abrupt lowering of the temperature by 2 °C (Rasmussen et al., 2014). This sudden decrease in temperature likely favored a readvance of the LIS margin, before resuming its slow retreat as the temperature gradually increased again. The presence of the moraine indicating stagnation at the fjord mouth is consistent with the relatively cold conditions across Baffin Bay at the end of the Younger Dryas (Buizert et al., 2014; Rasmussen et al., 2014) that promoted a positive mass balance and possibly counteracted ice loss by calving at the ice margin.

Alternatively, the early Holocene was marked by warmer atmospheric temperature around the Baffin Bay region, which favored extensive ice margin retreat (Pendleton et al., 2019; Lesnek et al., 2020). While temperatures were generally warm during the Holocene, cold spells were recorded in different proxies (i.e., Axford et al., 2009; Rasmussen et al., 2014) and appear to have favored ice margin stabilizations in Clyde Inlet. This deglaciation model is in agreement with observations around Baffin Bay where widespread moraine deposition have been associated with cold-climate oscillations at ~11.3, ~10.4, ~9.3 and ~8.2 ka (Young et al., 2020; Lesnek et al., 2020).

Inflow of subsurface water might have been an additional contributor to retreat rates in our study area through deglaciation. The intrusion of subsurface warm water have provoked accelerated melting and enhanced ice-margin retreat in modern-day marine-terminating glaciers (e.g., Straneo et al., 2010; Jeong et al., 2016; Howe et al., 2019), as well as on the shelves and fjords of many formerly glaciated regions (e.g., Sheldon et al., 2016; Arndt et al., 2017; Batchelor et al., 2019a; Allaart et al., 2020). However, the Baffin Island Current incorporates colder Arctic water from the CAA and Nares Strait (Tang et al., 2004; Münchow et al., 2015), therefore lowering the layer of warmer subsurface water. A reduction in the depth of warmer currents would weaken its influence on ice retreat along the Baffin shelf, in particular for the shallower Clyde Trough. Moreover, the shallow fjord-mouth sill (<200 m) probably prevented subsurface warm water from entering the fjord and triggering a catastrophic retreat. It is therefore unlikely that inflow of warmer currents had a major influence on the retreat of the CIS.

Although external forcing played an unequivocal role in the deglaciation of Clyde Inlet, the variability in retreat patterns when compared to other neighbouring fjord-cross-shelf trough systems indicates a local control on LIS margin oscillations.

5.2.2. Fjord/trough geometry controlling ice margin stabilization

Local-scale topography appears to have been a key factor in controlling the location of stabilizations during the retreat of the CIS. Depositional wedges and related stabilizations have been noted where topographic constrictions, highs and/or bends in the trough orientation occur. Although most topographic controls in the trough are bedrock-influenced, older GZWs might have produced a pinning point adequate enough to help the ice margin stabilize in the outer trough at the LGM (Fig. 7). Acting as a topographic high, these older GZWs restrained the LIS from flowing farther seaward regardless of the wider diffluent bed morphology by increasing the basal drag exerted on the ice stream (Dowdeswell and Fugelli, 2012; Batchelor and Dowdeswell, 2015; Hogan et al.,

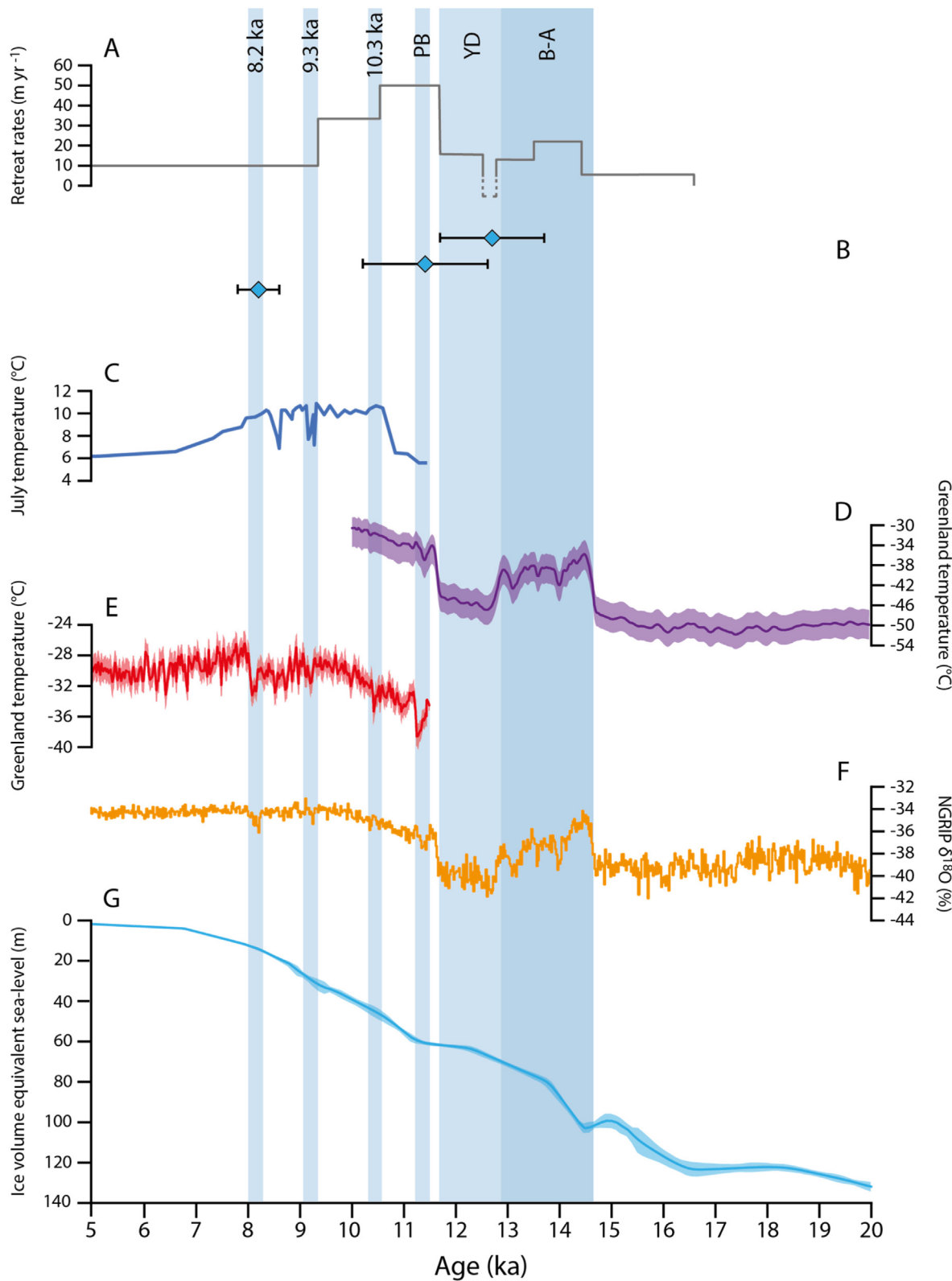


Fig. 11. (A) Average retreat rates between stabilizations in the Clyde fjord-cross-shelf trough system. The dashed line represents the uncertainties regarding the length and magnitude of the ice margin readvance during the Younger Dryas. (B) Exposure ages of moraine ridges along Clyde Inlet from Briner et al. (2007), recalculated using the Baffin Bay production rate (Young et al., 2013). (C) Chironomid-derived July temperature reconstruction from Lake CF8, eastern Baffin Island (dark blue; Axford et al., 2009). (D) Greenland mean-annual temperatures reconstructed using gas-phase $\delta^{15}\text{N}-\text{N}_2$ measurements (purple - ±1 σ ; Buizert et al., 2014). (E) Greenland mean-annual temperatures reconstructed using gas-phase $\Delta\text{Ar}-\text{N}_2$ measurements (red - ±2 σ ; Kleman et al., 2010). (F) $\delta^{18}\text{O}$ record from NGRIP project (orange; Rasmussen et al., 2014). (G) Ice volume equivalent sea-level (blue - ±1 σ ; Lambeck et al., 2014). Vertical bars represent cold and warm intervals discussed in the text. B–A: Bølling–Allerød; YD: Younger Dryas; PB: Preboreal.

2016; Bart et al., 2017; Danielson and Bart, 2019; Greenwood et al., 2021; Ottesen et al., 2022). A bend in the trough orientation, corresponding to a change in bedrock lithology, possibly further contributed to the formation of the morainal bank by enhancing lateral drag on the sides of the glacier (Syvitski and Shaw, 1995; Lyså and Vorren, 1997; Laberg et al., 2009; Jamieson et al., 2012, 2014; Ó Cofaigh et al., 2014; Bradwell et al., 2019). The relatively shallower depths compared to other cross-shelf trough systems of northeastern Baffin Island probably restricted the area of the ice front in contact with the ocean, resulting in a slower deglaciation in the middle trough as observed in similar settings (Arndt et al., 2017; Jakobsson et al., 2018). The shallower depths likely contributed to the slower deglaciation pattern observed across the retrograde slope of the mid- and inner trough following the YD readvance.

In contrast, deeper water in the fjord may have favored the acceleration in ice retreat (>50 m/year). Loss of contact with vertical pinning point reduces drag which, in turn, increases mass flow and iceberg calving rates (Syvitski and Shaw, 1995; Jamieson et al., 2014; Batchelor et al., 2019a). Coupled with the generally warmer atmosphere temperature of the early Holocene, it created an ideal setting for an enhanced retreat rate of the LIS in Clyde Inlet. However, cold events probably provoked intervening stabilizations of the ice margin in Clyde Inlet, while the fjord geometry influenced the location of most stabilizations. The outer fjord moraine is located at a pinning point created by multiple islands at the confluence of Clyde Inlet and Inugsuitt Fjord. This pinning-point allowed the ice margin to anchor and stabilize on the topographic high between islands. The location of the middle fjord moraine at the confluence of Clyde Inlet and Cormack Arm suggests, however, the influence of a funnel-shaped constriction of the ice (i.e., Syvitski and Shaw, 1995; Brouard and Lajeunesse, 2019a). Other ice-margin stabilizations in the inner fjord occurred at bends and lateral constrictions of the fjord width because of enhanced lateral-drag (Jamieson et al., 2012; Åkesson et al., 2018; Batchelor et al., 2019a; Brouard and Lajeunesse, 2019a). It must be emphasized here that not all constrictions or bends are associated with a stabilization in the fjord, as climate is likely the main driver for initiating a slow-down of the ice retreat.

6. Conclusions

The combination of multibeam bathymetry imagery, acoustic and seismic profiles, as well as sediment cores collected in the Clyde Inlet fjord-cross-shelf trough system provide new insights into the extent and retreat patterns of the Laurentide Ice Sheet margin on northeastern Baffin Island during the Last Glacial cycle. Key results of this analysis are:

- The LIS margin probably did not extend all the way across the continental shelf in Clyde Trough during the LGM; its maximal extent was rather located some 10 km from the shelf break. However, as the absence of direct dating on the upper continental slope restrains us from providing confirmation, the question of the maximal extent of the LIS in Clyde Trough remains open.
- Deglaciation on the shelf was temporally constrained to the late glacial (16–11.7 ka). It was marked by an initial collapse of the Clyde ice shelf and rapid LIS margin retreat, followed by a slow retreat of the ice margin with intervening stabilizations and interrupted by a readvance during the Younger Dryas. This deglaciation pattern differs from observations made in other troughs of northeastern Baffin Island shelf, where it appears to have been more rapid and episodic with wider spaced GZWs.
- Similarly to other fjords of northeastern Baffin Island, the ice margin retreated into Clyde Inlet in a less catastrophic pattern

than previously proposed for the early Holocene (11.7–8 ka). Our age constraints support earlier works that suggest numerous ice margin stabilizations during the early Holocene, which could be linked to cold climate events at ~10.3, ~9.3 and ~8.2 ka. The retreat was, however, rapid between successive stabilizations due to greater water depths in the fjord.

- Climate was the main driver of deglaciation in the Clyde area, as the available chronology suggests that most stabilizations coincided with regional-wide cooling events. Deglaciation patterns in the Clyde area were strongly influenced by topography, as ice margin stabilizations occurred at pinning points in both the trough and fjord. Oceanic forcing, such as global sea level fluctuations and ocean temperatures, appears to only have had a secondary influence on rates of ice sheet retreat in the Clyde fjord-cross-shelf trough system.

These results highlight the variability of ice-sheet retreat patterns and controls along a single high Arctic fjord-cross-shelf trough system, and from one system to another. However, uncertainties remain concerning the timing of ice margin stabilizations on northeastern Baffin Island, especially on the continental shelf. Future work on Baffin Island fjord-cross-shelf trough systems should therefore focus on establishing a robust deglaciation chronology combining both marine- and terrestrial-based investigations, which would improve our knowledge on factors controlling glacier behaviour and provide key information for testing numerical simulations on climate and predicting future ice mass loss in a warming world.

Author contributions

POC conceived the study and initiated this project in cooperation with PL and JFG. POC interpreted the geophysical data sets, conducted the sediment core analysis, wrote the paper and prepared the figures. PL, JFG, BD, CG, DH, and EB were involved in the discussion of the data and contributed to the final version of this paper.

Declaration of competing interest

The authors declare that they have no known competing financial interests or personal relationships that could have appeared to influence the work reported in this paper.

Data availability

The multibeam bathymetric data collected in 2017 during expedition MSM66 have been deposited in the PANGAEA repository (<https://doi.org/10.1594/PANGAEA.902341>). The multi-beam bathymetric data from ArcticNet cruises can be visualized on the Université Laval Géoindex + website (<http://geoindex-plus.bibl.ulaval.ca>). The Parasound profiles collected in 2017 during expedition MSM66 have been deposited in the PANGAEA repository (<https://doi.pangaea.de/10.1594/PANGAEA.944843>). The seismic reflection data along with the acquisition specifics are available on the Marine Data Holding public repository of National Resources Canada (<http://georgratis.gc.ca>).

Acknowledgments

We are thankful to the captains, crews and scientific participants on the different cruises for their help and support during the expeditions. This project was funded by the ArcticNet Network of Centers of Excellence, Natural Sciences and Engineering Research Council of Canada (NSERC) and Sentinelle Nord (Apogée Canada)

grants to PL, the *Deutsche Forschungsgemeinschaft* (DFG) grants to BD, CG and DH for ship-time and to DH for the International Research Training Group "ArcTrain" (IRTG 1904), as well as Université de Strasbourg grants to POC. We are grateful to *ArcTrain Canada* for providing financial support to this project. This study was supported by *Fonds québécois de la recherche sur la nature et les technologies* (FRQNT) through a travel grant to POC allowing sediment core analysis at the Center for Marine Environmental Sciences (MARUM – University of Bremen). We also thank Jens Weiser and Thomas Westerhold for their help with laboratory work. This paper was greatly improved by detailed and constructive comments by O. Bourgeois, C. Ó Cofaigh and D. B. Praeg, as well as formal reviews by E. L. King, one anonymous reviewer and the handling editor Antje Voelker.

References

- Aarseth, I., Austbø, P.K., Risnes, H., 1997. Seismic stratigraphy of Younger Dryas ice-marginal deposits in western Norwegian fjords. *Nor. Geol. Tidsskr.* 77 (2), 65–85.
- Akesson, H., Nisancioglu, K.H., Nick, F.M., 2018. Impact of fjord geometry on grounding line stability. *Front. Earth Sci.* 71, 1–16.
- Allaart, L., Müller, J., Schomacker, A., Rydningen, T.A., Hákansson, L., Kjellman, S.E., Mollenhauer, G., Forwick, M., 2020. Late Quaternary glacier and sea-ice history of northern Wijdefjorden, Svalbard. *Boreas* 49 (3), 417–437.
- Andrews, J.T., Drapier, L., 1967. Radiocarbon dates obtained through Geographical Branch field observations. *Geogr. Bull.* 9 (2), 115–162.
- Andrews, J.T., Ives, J.D., 1978. Cockburn" nomenclature and the late quaternary history of the eastern Canadian arctic. *Arct. Alp. Res.* 10 (3), 617–633.
- Andrews, J.T., Barnett, D., 1979. Holocene (Neoglacial) moraine and proglacial lake chronology, Barnes ice cap, Canada. *Boreas* 8 (3), 341–358.
- Andrews, J.T., Kirby, M.E., Aksu, A., Barber, D.C., Meese, D., 1998. Late Quaternary detrital carbonate (DC-) layers in Baffin Bay marine sediments (67°–74° N): correlation with Heinrich events in the North Atlantic? *Quat. Sci. Rev.* 17 (12), 1125–1137.
- Andrews, J.T., Dyke, A.S., 2007. Glaciations: late quaternary in North America. In: Elias, S.A. (Ed.), *Encyclopedia of Quaternary Science*. Elsevier, Amsterdam, pp. 1095–1101.
- Arndt, J.E., Jokat, W., Dorschel, B., 2017. The last glaciation and deglaciation of the Northeast Greenland continental shelf revealed by hydro-acoustic data. *Quat. Sci. Rev.* 160, 45–56.
- Arosio, R., Dove, D., Cofaigh, C.Ó., Howe, J.A., 2018. Submarine deglacial sediment and geomorphological record of southwestern Scotland after the Last Glacial Maximum. *Mar. Geol.* 403, 62–79.
- Axford, Y., Briner, J.P., Cooke, C.A., Francis, D.R., Michelutti, N., Miller, G.H., Smol, J.P., Thomas, E.K., Wilson, C.R., Wolfe, A.P., 2009. Recent changes in a remote Arctic lake are unique within the past 200,000 years. *Proc. Natl. Acad. Sci. USA* 106 (44), 18443–18446.
- Barnett, D.M., Holdsworth, G., 1974. Origin, morphology, and chronology of sub-lacustrine moraines, generator lake Baffin island, northwest territories, Canada. *Can. J. Earth Sci.* 11 (3), 380–408.
- Bart, P.J., Anderson, J.B., Nitsche, F., 2017. Post-LGM grounding-line positions of the bindschadler paleo ice stream in the ross sea embayment, Antarctica. *J. Geophys. Res.: Earth Surf.* 122 (10), 1827–1844.
- Batchelor, C.L., Dowdeswell, J.A., 2015. Ice-sheet grounding-zone wedges (GZW)s on high-latitude continental margins. *Mar. Geol.* 363, 65–92.
- Batchelor, C.L., Dowdeswell, J.A., 2016. Lateral shear-moraines and lateral marginal-moraines of palaeo-ice streams. *Quat. Sci. Rev.* 151, 1–26.
- Batchelor, C.L., Dowdeswell, J.A., Rignot, E., 2018. Submarine landforms reveal varying rates and styles of deglaciation in North-West Greenland fjords. *Mar. Geol.* 402, 60–80.
- Batchelor, C.L., Dowdeswell, J.A., Rignot, E., Millan, R., 2019a. Submarine moraines in Southeast Greenland fjords reveal contrasting outlet-glacier behaviour since the Last Glacial Maximum. *Geophys. Res. Lett.* 46, 3279–3286.
- Batchelor, C.L., Margold, M., Krapp, M., Murton, D.K., Dalton, A.S., Gibbard, P.L., Stokes, C.R., Murton, J.B., Manica, A., 2019b. The configuration of Northern Hemisphere ice sheets through the Quaternary. *Nat. Commun.* 10 (1), 1–10.
- Bjarnadóttir, L.R., Rüther, D.C., Winsborrow, M., Andreassen, K., 2012. Grounding-line dynamics during the last deglaciation of Kveithola, W Barents Sea, as revealed by seabed geomorphology and shallow seismic stratigraphy. *Boreas* 42 (1), 84–107.
- Boulton, G.S., 1986. Push-moraines and glacier-contact fans in marine and terrestrial environments. *Sedimentology* 33 (5), 677–698.
- Bradwell, T., Small, D., Fabel, D., Smedley, R.K., Clark, C.D., Saher, M.H., Callard, S.L., Chiverrell, R.C., Dove, C., Moreton, S.G., Roberts, D.H., Duller, G.A.T., Ó Cofaigh, C., 2019. Ice-stream demise dynamically conditioned by trough shape and bed strength. *Sci. Adv.* 5 (4), eaau1380.
- Briner, J.P., Miller, G.H., Davis, P.T., Finkel, R.C., 2005. Cosmogenic exposure dating in arctic glacial landscapes: implications for the glacial history of northeastern Baffin Island, Arctic Canada. *Can. J. Earth Sci.* 42, 67–84.
- Briner, J.P., Miller, G.H., Davis, P.T., Finkel, R.C., 2006. Cosmogenic radionuclides from fiord landscapes support differential erosion by overriding ice sheets. *Geol. Soc. Am. Bull.* 118, 406–420.
- Briner, J.P., Overeem, I., Miller, G.H., Finkel, R.C., 2007. The deglaciation of Clyde inlet, northeastern Baffin island, arctic Canada. *J. Quat. Sci.* 22, 223–232.
- Briner, J.P., Bini, A.C., Anderson, R.S., 2009a. Rapid early Holocene retreat of a Laurentide outlet glacier through an Arctic fjord. *Nat. Geosci.* 2, 496–499.
- Briner, J.P., Davis, P.T., Miller, G.H., 2009b. Latest pleistocene and Holocene glaciation of Baffin island, arctic Canada: key patterns and chronologies. *Quat. Sci. Rev.* 28 (21–22), 2075–2087.
- Briner, J.P., Cuzzone, J.K., Badgeley Young, N.E., Steig, E.J., Morlighem, M., Schlegel, N.J., Hakim, G.J., Schaefer, J.M., Johnson, J.V., Lesnek, A.J., Thomas, E.K., J. Allan, E., Bennike, O., Cluett, A., Csatho, B., de Vernal, A., Downs, J., Larour, E., Nowicki, S., 2020. Rate of mass loss from the Greenland Ice Sheet will exceed Holocene values this century. *Nature* 586 (7827), 70–74.
- Brouard, E., Lajeunesse, P., 2017. Maximum extent and decay of the Laurentide ice sheet in western Baffin bay during the last glacial episode. *Sci. Rep.* 7 (1), 10711.
- Brouard, E., Lajeunesse, P., 2019a. Glacial to postglacial submarine landform assemblages in fjords of northeastern Baffin Island. *Geomorphology* 330, 40–56.
- Brouard, E., Lajeunesse, P., 2019b. Submarine geomorphology of the northeastern Baffin Island fjords and cross-shelf troughs. *J. Maps* 15, 662–676.
- Brouard, E., Lajeunesse, P., 2019c. Ice-stream flow switching by up-ice propagation of instabilities along glacial marginal troughs. *Cryosphere* 13 (3), 981–996.
- Callard, S.L., Ó Cofaigh, C., Benetti, S., Chiverrell, R.C., Van Landeghem, K.J.J., Saher, M.H., Gales, J.A., Small, D., Clark, C.D., Livingstone, S.J., Fabel, D., Moreton, S.G., 2018. Extent and retreat history of the Barra Fan Ice Stream offshore western Scotland and northern Ireland during the last glaciation. *Quat. Sci. Rev.* 201, 280–302.
- Buizert, C., Gkinis, V., Severinghaus, J.P., He, F., Lecavalier, B.S., Kindler, P., Leuenberger, M., Carlson, A.E., Vinther, B., Masson-Delmotte, V., White, J.W.C., Liu, Z., Otto-Bliesner, B., Brook, E.J., 2014. Greenland temperature response to climate forcing during the last deglaciation. *Science* 345 (6201), 1177–1180.
- Callard, S.L., Cofaigh, C.Ó., Benetti, S., Chiverrell, R.C., Van Landeghem, K.J., Saher, M.H., Livingstone, S.J., Clark, C.D., Fabel, D., Moreton, S.G., 2020. Oscillating retreat of the last British-Irish Ice Sheet on the continental shelf offshore Galway Bay, western Ireland. *Mar. Geol.* 420, 106087.
- Carlson, A.E., 2009. Geochemical constraints on the Laurentide Ice Sheet contribution to meltwater pulse 1A. *Quat. Sci. Rev.* 28, 1625–1630.
- Clark, C.D., 1993. Mega-scale glacial lineations and cross-cutting ice-flow landforms. *Earth Surf. Process. Landforms* 18 (1), 1–29.
- Clark, C.D., Tulaczyk, S.M., Stokes, C.R., Canals, M., 2003. A groove-ploughing theory for the production of mega-scale glacial lineations, and implications for ice-stream mechanics. *J. Glaciol.* 49 (165), 240–256.
- Couette, P.-O., Lajeunesse, P., Ghienne, J.-F., Dorschel, B., Gebhardt, C., Hebbeln, D., Brouard, E., 2022. Evidence for an extensive ice shelf in northern Baffin bay during the last glacial maximum. *Communications Earth and Environment* 3 (1), 1–12.
- Crump, S.E., Young, N.E., Miller, G.H., Pendleton, S.L., Tulenko, J.P., Anderson, R.S., Briner, J.P., 2020. Glacier expansion on Baffin Island during early Holocene cold reversals. *Quat. Sci. Rev.* 241, 106419.
- Dalton, A.S., Margold, M., Stokes, C.R., Tarasov, L., Dyke, A.S., Adams, R.S., Allard, S., Arends, H.E., Atkinson, N., Attig, J.W., Barnett, P.J., Barnett, R.L., Batterson, M., Bernatchez, P., Borns, H.W., Breckenridge, A., Briner, J.P., Brouard, E., Campbell, J.E., Carlson, A.E., Clague, J.J., Curry, B.B., Daigneault, R.A., Dubé-Loubert, H., Easterbrook, D.J., Franzl, D.A., Friedrich, H.G., Funder, S., Gauthier, M.S., Gowan, A.S., Harris, K.L., Hétu, B., Hooyer, T.S., Jennings, C.E., Johnson, M.D., Kehew, A.E., Kelley, S.E., Kerr, D., King, E.L., Kjeldsen, K.K., Knaeble, A.R., Lajeunesse, P., Lakeman, T.R., Lamotte, M., Larson, P., Lavoie, M., Loope, H.M., Lowell, T.V., Lusardi, B.A., Manz, L., McMartin, I., Nixon, F.C., Occhietti, S., Parkhill, M.A., Piper, D.J.W., Pronk, A.G., Richard, P.J.H., Ridge, J.C., Ross, M., Roy, M., Seaman, A., Shaw, J., Stea, R.R., Teller, J.T., Thompson, W.B., Thorleifson, L.H., Utting, D.J., Veillette, J.J., Ward, B.C., Weddle, T.K., Wright, H.E., 2020. An updated radiocarbon-based ice margin chronology for the last deglaciation of the North American Ice Sheet Complex. *Quat. Sci. Rev.* 234, 106223.
- Danielson, M., Bart, P.J., 2019. Topographic control on the post-LGM grounding zone locations of the west antarctic ice sheet in the whales deep basin, eastern ross sea. *Mar. Geol.* 407, 248–260.
- Davis, P.T., Briner, J.P., Coulthard, R.D., Finkel, R.W., Miller, G.H., 2006. Preservation of Arctic landscapes overridden by cold-based ice sheets. *Quat. Res. (Orlando)* 65, 156–163.
- De Angelis, H., Kleman, J., 2007. Palaeo-ice streams in the foxe/baffin sector of the Laurentide ice sheet. *Quat. Sci. Rev.* 26, 1313–1331.
- Dorschel, B., Allan, E., Bartels, M., Campbell, C., Couette, P.O., Diekamp, V., Dreutter, S., Duboc, Q., Geils, J., Greco, M., Lenz, K.F., Lübben, B., Lütjens, M., Madaj, L., Perez, L., Recinos, B., Saini, J., Schade, T., Täuber, F., Ulner, L.C., Warneke, F., Weiser, J., 2017. WESTBAFF reconstruction of the Laurentide ice sheet drainage into the northwest Baffin bay and the palaeoceanography of the west Baffin bay - cruise No. MSM66. In: Nuuk (Greenland) - Reykjavik (Iceland), Maria S. Merian Berichte. Gutachterpanel Forschungsschiffe, Bonn, p. 52. July 22 – August 28, 2017.
- Dowdeswell, J.A., Whittington, R.J., Marienfeld, P., 1994. The origin of massive diamicton facies by iceberg rafting and scouring, Scoresby Sund, East Greenland. *Sedimentology* 41, 21–35.
- Dowdeswell, J.A., Whittington, R.J., Jennings, A.E., Andrews, J.T., Mackensen, A.,

- Marienfeld, P., 2000. An origin for laminated glacimarine sediments through sea-ice build-up and suppressed iceberg rafting. *Sedimentology* 47, 557–576.
- Dowdeswell, J.A., Ottesen, D., Evans, J., Cofaigh, C.O., Anderson, J.B., 2008. Submarine glacial landforms and rates of ice-stream collapse. *Geology* 36 (10), 819–822.
- Dowdeswell, J.A., Fugelli, E.M.G., 2012. The seismic architecture and geometry of grounding-zone wedges formed at the marine margins of past ice sheets. *Geol. Soc. Am. Bull.* 124 (11–12), 1750–1761.
- Dowdeswell, J.A., Vásquez, M., 2013. Submarine landforms in the fjords of southern Chile: implications for glacimarine processes and sedimentation in a mild glacier-influenced environment. *Quat. Sci. Rev.* 64, 1–19.
- Dowdeswell, J.A., Hogan, K.A., Cofaigh, C.O., Fugelli, E.M.G., Evans, J., Noormets, R., 2014. Late Quaternary ice flow in a West Greenland fjord and cross-shelf trough system: submarine landforms from Rink Isbrae to Uummannaq shelf and slope. *Quat. Sci. Rev.* 92, 292–309.
- Dowdeswell, J.A., Hogan, K.A., Arnold, N.S., Mugford, R.I., Wells, M., Hirst, J.P.P., Decalf, C., 2015. Sediment-rich meltwater plumes and ice-proximal fans at the margins of modern and ancient tidewater glaciers: observations and modelling. *Sedimentology* 62 (6), 1665–1692.
- Dowdeswell, J.A., Todd, B.J., Dowdeswell, E.K., Batchelor, C.L., 2016a. Ice-sculpted bedrock in channels of the Canadian arctic Archipelago. In: Dowdeswell, J.A., Canals, M., Jakobsson, M., Todd, B.J., Dowdeswell, E.K., Hogan, K. (Eds.), *Atlas of Submarine Glacial Landforms: Modern, Quaternary and Ancient*, vol. 46. Geological Society, London, Memoirs, pp. 59–60.
- Dowdeswell, J.A., Canals, M., Jakobsson, M., Todd, B.J., Dowdeswell, E.K., Hogan, K.A., 2016b. The variety and distribution of submarine glacial landforms and implications for ice-sheet reconstruction. In: Dowdeswell, J.A., Canals, M., Jakobsson, M., Todd, B.J., Dowdeswell, E.K., Hogan, K. (Eds.), *Atlas of Submarine Glacial Landforms: Modern, Quaternary and Ancient*, vol. 46. Geological Society, London, Memoirs, pp. 89–90.
- Dyke, A.S., Morris, T.F., 1988. Drumlin fields, dispersal trains, and ice streams in Arctic Canada. *Can. Geogr.* 32 (1), 86–90.
- Dyke, A.S., Andrews, J.T., Clark, P.U., England, J.H., Miller, G.H., Shaw, J., Veillette, J.J., 2002. The Laurentide and innuitian ice sheets during the last glacial maximum. *Quat. Sci. Rev.* 21, 9–31.
- Dyke, A.S., 2004. An outline of North American deglaciation with emphasis on central and northern Canada. *Dev. Quat. Sci.* 2, 373–424.
- Evans, D.J., Rea, B.R., 1999. Geomorphology and sedimentology of surging glaciers: a land-systems approach. *Ann. Glaciol.* 28, 75–82.
- Fader, G.B., Amos, C.L., Best, M.A., Cameron, G.D.M., Jennings, A., Josenhans, H., MacLean, B., Powell, C., Sonnichsen, G., 1989. Quaternary Geology of the Continental Margin of Eastern Canada. Geological Survey of Canada, Map, 000, 1705A Scale 1:5,000.
- Favier, L., Durand, G., Cornford, S.L., Gudmundsson, G.H., Gagliardini, O., Gillet-Chaulet, F., Zwinger, T., Payne, A.J., Le Brocq, A.M., 2014. Retreat of Pine Island Glacier controlled by marine ice-sheet instability. *Nat. Clim. Change* 4 (2), 117–121.
- Flink, A.E., Noormets, R., 2018. Submarine glacial landforms and sedimentary environments in Vaigattbogen, northeastern Spitsbergen. *Mar. Geol.* 402, 244–263.
- Gilbert, R., Naldrett, D.L., Horvath, V.V., 1990. Holocene sedimentary environment of Cambridge fiord, Baffin island, northwest territories. *Can. J. Earth Sci.* 27, 271–280.
- Greenwood, S.L., Simkins, L.M., Winsborrow, M.C., Bjarnadóttir, L.R., 2021. Exceptions to bed-controlled ice sheet flow and retreat from glaciated continental margins worldwide. *Sci. Adv.* 7 (3), eabb6291.
- Harrison, S., Smith, D.E., Glasser, N.F., 2018. Late Quaternary meltwater pulses and sea level change. *J. Quat. Sci.* 34, 1–15.
- Heaton, T.J., Köhler, P., Butzin, M., Bard, E., Reimer, R.W., Austin, W.E., Bronk Ramson, C., Grottes, P.M., Hughen, K.A., Kromer, B., Reimer, P.J., Adkins, J., Burke, A., Cook, M.S., Olsen, J., Skinner, L.C., 2020. Marine20—the marine radiocarbon age calibration curve (0–55,000 cal BP). *Radiocarbon* 62 (4), 779–820.
- Heaton, T.J., Bard, E., Ramsey, C.B., Butzin, M., Hatté, C., Hughen, K.A., Köhler, P., Reimer, P.J., 2022. A response to community questions on the Marine20 radiocarbon age calibration curve: marine reservoir ages and the calibration of ^{14}C samples from the oceans. *Radiocarbon* 1–27.
- Hiscott, R.N., Aksu, A.E., Nielsen, O.B., 1989. Provenance and dispersal patterns, Pliocene-Pleistocene section at site 645, Baffin Bay. *Proc. Ocean Drill. Program Sci. Results* 105, 31–52. <https://doi.org/10.2973/odp.proc.sr.105.117.1989>.
- Hodgson, D.A., Graham, A.G., Griffiths, H.J., Roberts, S.J., Cofaigh, C.O., Bentley, M.J., Evans, D.J., 2014. Glacial history of sub-Antarctic South Georgia based on the submarine geomorphology of its fjords. *Quat. Sci. Rev.* 89, 129–147.
- Hogan, K.A., Cofaigh, C.O., Jennings, A.E., Dowdeswell, J.A., Hiemstra, J.F., 2016. Deglaciation of a major palaeo-ice stream in Disko Trough, west Greenland. *Quat. Sci. Rev.* 147, 5–26.
- Hogan, K.A., Jakobsson, M., Mayer, L., Reilly, B.T., Jennings, A.E., Stoner, J.S., Nielsen, T., Andresen, K.J., Nørmark Heirman, K.A., Kamla, E., Jerram, K., Stranne, C., Mix, A., 2020. Glacial sedimentation, fluxes and erosion rates associated with ice retreat in Petermann Fjord and Nares Strait, north-west Greenland. *Cryosphere* 14, 261–286.
- Howe, J.A., Husum, K., Inall, M.E., Coogan, J., Luckman, A., Arosio, R., Abernethy, C., Verchili, D., 2019. Autonomous underwater vehicle (AUV) observations of recent tidewater glacier retreat, western Svalbard. *Mar. Geol.* 417, 106009.
- Hughes, P.D., Gibbard, P.L., Ehlers, J., 2013. Timing of glaciation during the last glacial cycle: evaluating the concept of a global 'Last Glacial Maximum' (LGM). *Earth Sci. Rev.* 125, 171–198.
- Jackson, G.D., Blusson, S.L., Crawford, W.J., Davidson, A., Morgan, W.C., Kranck, E.H., Riley, G., Eade, K.E., 1984. Geology, Clyde River, district of Franklin: geological survey of Canada. A Series Map 1582A, scale 1, 250.
- Jackson, R., Carlson, A.E., Hillaire-Marcel, C., Wacker, L., Vogt, C., Kucera, M., 2017. Asynchronous instability of the North American-Arctic and Greenland ice sheets during the last deglaciation. *Quat. Sci. Rev.* 164, 140–153.
- Jakobsson, M., Anderson, J.B., Nitsche, F.O., Dowdeswell, J.A., Gyllencreutz, R., Kirchner, N., Mohammad, R., O'Regan, M., Alley, R.B., Anandakrishnan, S., Eriksson, B., Kirchner, A., Fernandez, R., Stoddorf, T., Minzoni, R., Majewski, W., 2011. Geological record of ice shelf break-up and grounding line retreat, Pine Island Bay, west Antarctica. *Geology* 39, 691–694.
- Jakobsson, M., Mayer, L., Coakley, B., Dowdeswell, J.A., Forbes, S., Fridman, B., Hodgesdal, H., Noormets, R., Pedersen, R., Rebisco, M., Schenke, H.W., Zarayskaya, Y., Accettella, D., Armstrong, A., Anderson, R.M., Bienhoff, P., Camerlenghi, A., Church, I., Edwards, M., Gardner, J.V., Hall, J.K., Hell, B., Hestvik, O., Kristoffersen, Y., Marcussen, C., Mohammad, R., Mosher, D., Nghiêm, S.V., Pedrosa, M.T., Travaglini, P.G., Weatherall, P., 2014. The international bathymetric Chart of the Arctic Ocean (IBCAO) version 3.0. *Geophys. Res. Lett.* 39 (12), L12609.
- Jakobsson, M., Hogan, K.A., Mayer, L.A., Mix, A., Jennings, A., Stoner, J., Eriksson, B., Jerram, K., Mohammad, R., Pearce, C., Reilly, B., Stranne, C., 2018. The Holocene retreat dynamics and stability of Petermann Glacier in northwest Greenland. *Nat. Commun.* 9 (1), 2104.
- Jamieson, S.S., Vieli, A., Cofaigh, C.O., Stokes, C.R., Livingstone, S.J., Hillenbrand, C.D., 2014. Understanding controls on rapid ice-stream retreat during the last deglaciation of Marguerite Bay, Antarctica, using a numerical model. *J. Geophys. Res. Earth Surf.* 119 (2), 247–263.
- Jamieson, S.S., Vieli, A., Livingstone, S.J., Cofaigh, C.O., Stokes, C., Hillenbrand, C.D., Dowdeswell, J.A., 2012. Ice-stream stability on a reverse bed slope. *Nat. Geosci.* 5 (11), 799–802.
- Jenner, K.A., Campbell, D.C., Piper, D.J.W., 2018. Along-slope variations in sediment lithofacies and depositional processes since the Last Glacial Maximum on the northeast Baffin margin, Canada. *Mar. Geol.* 405, 92–107.
- Jennings, A.E., 1993. The quaternary history of Cumberland Sound, southeastern Baffin island: the marine evidence. *Géogr. Phys. Quaternaire* 47 (1), 21–42.
- Jennings, A.E., Sheldon, C., Cronin, T.M., Francus, P., Stoner, J., Andrews, J., 2011. The Holocene history of Nares Strait: transition from glacial bay to arctic-atlantic throughflow. *Oceanography* 24, 26–41.
- Jennings, A.E., Walton, M.E., O'Cofaigh, C.O.L.M., Kilfeather, A., Andrews, J.T., Ortiz, J.D., de Vernal, A., Dowdeswell, J.A., 2014. Paleoenvironments during younger dryas-E arly Holocene retreat of the Greenland ice sheet from outer Disko Trough, central west Greenland. *J. Quat. Sci.* 29 (1), 27–40.
- Jennings, A.E., Andrews, J.T., Cofaigh, C.O., Onge, G.S., Sheldon, C., Belt, S.T., Cabedo-Sanz, P., Hillaire-Marcel, C., 2017. Ocean forcing of ice sheet retreat in central west Greenland from LGM to the early Holocene. *Earth Planet. Sci. Lett.* 472, 1–13.
- Jennings, A.E., Andrews, J.T., Cofaigh, C.O., St-Onge, G., Belt, S., Cabedo-Sanz, P., Pearce, C., Hillaire-Marcel, C., Campbell, D.C., 2018. Baffin Bay paleoenvironments in the LGM and HS1: resolving the ice-shelf question. *Mar. Geol.* 402, 5–16.
- Jeong, S., Howat, I.M., Bassis, J.N., 2016. Accelerated ice shelf rifting and retreat at Pine Island glacier, west Antarctica. *Geophys. Res. Lett.* 43 (22), 11–720.
- Joughin, I., Alley, R.B., Holland, D.M., 2012. Ice-sheet response to oceanic forcing. *Sci. Technol. Humanit.* 338 (6111), 1172–1176.
- King, L.H., 1976. Relict iceberg furrows on the Laurentian channel and western grand banks. *Can. J. Earth Sci.* 13 (8), 1082–1092.
- King, E.L., Hafslidason, H., Sejrup, H.P., Løvlie, R., 1998. Glacigenic debris flows on the North Sea Trough Mouth Fan during ice stream maxima. *Mar. Geol.* 152 (1–3), 217–246.
- Kleman, J., Jansson, K., De Angelis, H., Stroeve, A.P., Hattestrand, C., Alm, G., Glasser, N.F., 2010. North American Ice Sheet build-up during the last glacial cycle, 115–21 kyr. *Quat. Sci. Rev.* 29, 17–18.
- Laberg, J.S., Eilertsen, R.S., Vorren, T.O., 2009. The paleo-ice stream in Vestfjorden, north Norway, over the last 35 kyr: Glacial erosion and sediment yield. *Geol. Soc. Am. Bull.* 121 (3–4), 434–447.
- Lambeck, K., Rouby, H., Purcell, A., Sun, Y., Cambridge, M., 2014. Sea level and global ice volumes from the last glacial maximum to the Holocene. *Proc. Natl. Acad. Sci. USA* 111 (43), 15296–15303.
- Lesnek, A.J., Briner, J.P., Young, N.E., Cuzzone, J.K., 2020. Maximum southwest Greenland ice sheet recession in the early Holocene. *Geophys. Res. Lett.* 47 (1), e2019GL083164.
- Lévesque, Y., St-Onge, G., Lajeunesse, P., Desiage, P.A., Brouard, E., 2020. Defining the maximum extent of the Laurentide ice sheet in home bay (eastern Arctic Canada) during the last glacial episode. *Boreas* 49 (1), 52–70.
- Lewis, C.F.M., Todd, B.J., Sonnichsen, G.V., King, T., 2016. Iceberg-seabed interaction on northwestern makkovik bank, labrador shelf, Canada. In: Dowdeswell, J.A., Canals, M., Jakobsson, M., Todd, B.J., Dowdeswell, E.K., Hogan, K. (Eds.), *Atlas of Submarine Glacial Landforms: Modern, Quaternary and Ancient*, vol. 46. Geological Society, London, Memoirs, pp. 279–280.
- Li, G., Piper, D.J., Calvin Campbell, D., 2011. The quaternary Lancaster Sound trough-mouth fan, NW Baffin Bay. *J. Quat. Sci.* 26 (5), 511–522.
- Lin, Y., Hibbert, F.D., Whitehouse, P.L., Woodroffe, S.A., Purcell, A., Shennan, I., Bradley, S.L., 2021. A reconciled solution of Meltwater Pulse 1A sources using

- sea-level fingerprinting. *Nat. Commun.* 12, 1–11.
- Lindén, M., Möller, P., 2005. Marginal formation of De Geer moraines and their implications to the dynamics of grounding-line recession. *J. Quat. Sci.* 20 (2), 113–133.
- Løken, O.H., Hodgson, D.A., 1971. On the submarine geomorphology along the east coast of Baffin island. *Can. J. Earth Sci.* 8, 185–195.
- Lønne, I., 1995. Sedimentary facies and depositional architecture of ice-contact glaciomarine systems. *Sediment. Geol.* 98 (1–4), 13–43.
- Lowry, D.P., Golledge, N.R., Bertler, N.A., Jones, R.S., McKay, R., Stutz, J., 2020. Geologic controls on ice sheet sensitivity to deglacial climate forcing in the Ross Embayment, Antarctica. *Quaternary Science Advances* 1, 100002.
- Lyså, A., Vorren, T.O., 1997. Seismic facies and architecture of ice-contact submarine fans in high-relief fjords, Troms, Northern Norway. *Boreas* 26 (4), 309–328.
- MacLean, B., Blasco, S., Bennett, R., Clarke, J.H., Patton, E., 2016. Crag-and-tail features, amundsen gulf, Canadian arctic Archipelago. In: Dowdeswell, J.A., Canals, M., Jakobsson, M., Todd, B.J., Dowdeswell, E.K., Hogan, K. (Eds.), *Atlas of Submarine Glacial Landforms: Modern, Quaternary and Ancient*, vol. 46. Geological Society, London, Memoirs, pp. 53–54.
- Margold, M., Stokes, C.R., Clark, C.D., 2018. Reconciling records of ice streaming and ice margin retreat to produce a palaeogeographic reconstruction of the deglaciation of the Laurentide Ice Sheet. *Quat. Sci. Rev.* 189, 1–30.
- Margreth, A., Gosse, J.C., Dyke, A.S., 2017. Wisconsinan and early Holocene glacial dynamics of Cumberland Peninsula, Baffin island, arctic Canada. *Quat. Sci. Rev.* 168, 79–100.
- Miller, G.H., Andrews, J.T., Short, S.K., 1977. The last interglacial–glacial cycle, Clyde foreland, Baffin Island, NWT: stratigraphy, biostratigraphy, and chronology. *Can. J. Earth Sci.* 14 (12), 2824–2857.
- Miller, G.H., Wolfe, A.P., Steig, E.J., Sauer, P.E., Kaplan, M.R., Briner, J.P., 2002. The Goldilocks dilemma: big ice, little ice, or “just-right” ice. *Quat. Sci. Rev.* 22, 33–48.
- Miller, G.H., Wolfe, A.P., Briner, J.P., Sauer, P.E., Nesje, A., 2005. Holocene glaciation and climate evolution of Baffin island, arctic Canada. *Quat. Sci. Rev.* 24, 1703–1721.
- Münchow, A., Falkner, K.K., Melling, H., 2015. Baffin island and west Greenland current systems in northern Baffin bay. *Prog. Oceanogr.* 132, 305–317.
- Normandeau, A., Dietrich, P., Clarke, J.H., Van Wychen, W., Lajeunesse, P., Burgess, D., Ghienne, J.F., 2019. The Retreat Pattern of Glaciers Controls the Occurrence of Turbidity Currents on High-Latitude Fjord Deltas.
- Ó Cofaigh, C., Dowdeswell, J.A., 2001. Laminated sediments in glaciomarine environments: diagnostic criteria for their interpretation. *Quat. Sci. Rev.* 20 (13), 1411–1436.
- Ó Cofaigh, C., Dowdeswell, J.A., Evans, J., Larter, R.D., 2008. Geological constraints on Antarctic palaeo-ice-stream retreat. *Earth Surf. Process. Landforms* 33 (4), 513–525.
- Ó Cofaigh, C., Andrews, J.T., Jennings, A.E., Dowdeswell, J.A., Hogan, K.A., Kilfeather, A.A., Sheldon, C., 2013a. Glaciomarine lithofacies, provenance and depositional processes on a West Greenland trough-mouth fan. *J. Quat. Sci.* 28 (1), 13–26.
- Ó Cofaigh, C., Dowdeswell, J.A., Jennings, A.E., Hogan, K.A., Kilfeather, A., Hiemstra, J.F., Noormets, R., Evans, J., McCarthy, D.J., Andrews, J.T., Lloyd, J.M., Moros, M., 2013b. An extensive and dynamic ice sheet on the West Greenland shelf during the last glacial cycle. *Geology* 41 (2), 219–222.
- Ó Cofaigh, C., Davies, B.J., Livingstone, S.J., Smith, J.A., Johnson, J.S., Hocking, E.P., Hodgson, D.A., Anderson, J.B., Bentley, M.J., Canal, M., Domack, E., Dowdeswell, J.A., Evans, J., Glasser, N.F., Hillenbrand, C.-D., Larter, R.D., Roberts, S.J., Simms, A.R., 2014. Reconstruction of ice-sheet changes in the antarctic Peninsula since the last glacial maximum. *Quat. Sci. Rev.* 100, 87–110.
- Olsen, I.L., Rydningen, T.A., Forwick, M., Laberg, J.S., Husum, K., 2020. Last glacial ice sheet dynamics offshore NE Greenland – a case study from Store Koldewey Trough. *Cryosphere* 14 (12), 4475–4494.
- Olsen, I.L., Laberg, J.S., Forwick, M., Rydningen, T.A., Husum, K., 2022. Late weichselian and Holocene behavior of the Greenland ice sheet in the kejser franz josef fjord system, NE Greenland. *Quat. Sci. Rev.* 284, 107504.
- Osterman, L.E., Nelson, A.R., 1989. Latest Quaternary and Holocene paleoceanography of the eastern Baffin Island continental shelf, Canada: benthic foraminiferal evidence. *Can. J. Earth Sci.* 26 (11), 2236–2248.
- Ottesen, D., Rise, L., Knies, J., Olsen, L., Henriksen, S., 2005. The Vestfjorden-Trænadupjet palaeo-ice stream drainage system, mid-Norwegian continental shelf. *Mar. Geol.* 218, 175–189.
- Ottesen, D., Dowdeswell, J.A., Landvik, J.Y., Mienert, J., 2007. Dynamics of the Late Weichselian ice sheet on Svalbard inferred from high-resolution sea-floor morphology. *Boreas* 36, 286–306.
- Ottesen, D., Dowdeswell, J.A., Bellec, V.K., Bjarnadóttir, L.R., 2017. The geomorphic imprint of glacier surges into open-marine waters: examples from eastern Svalbard. *Mar. Geol.* 392, 1–29.
- Ottesen, D., Batchelor, C.L., Bjarnadóttir, L.R., Wiberg, D.H., Dowdeswell, J.A., 2022. Glacial landforms reveal dynamic ice-sheet behaviour along the mid-Norwegian margin during the last glacial-deglacial cycle. *Quat. Sci. Rev.* 285, 107462.
- Pendleton, S., Miller, G., Lifton, N., Young, N., 2019. Cryosphere response resolves conflicting evidence for the timing of peak Holocene warmth on Baffin Island, Arctic Canada. *Quat. Sci. Rev.* 216, 107–115.
- Pieńkowski, A.J., Coulthard, R.D., Furze, M.F.A., 2022. Revised marine reservoir offset (ΔR) values for molluscs and marine mammals from Arctic North America. *Boreas*. <https://doi.org/10.1111/bor.12606>.
- Powell, R.D., 1981. A model for sedimentation by tidewater glaciers. *Ann. Glaciol.* 2, 129–134.
- Powell, R.D., 1990. Glaciomarine processes at grounding-line fans and their growth to ice-contact deltas. In: Dowdeswell, J.A., Scourse, J.D. (Eds.), *Glaciomarine Environments: Processes and Sediments*, vol. 53. Geological Society, London, Special Publications, pp. 53–73, 1.
- Powell, R.D., Domack, E., 1995. Modern glacio marine environments. In: Menzies, J. (Ed.), *Glacial Environments: Volume I. Modern Glacial Environments: Processes, Dynamics and Sediments*. Butterworth-Heinemann, Oxford, pp. 445–486.
- Powell, R.D., Alley, R.B., 1997. Grounding-line systems: processes, glaciological inferences and the stratigraphic record. In: Barker, P.F., Cooper, A.C. (Eds.), *Geology and Seismic Stratigraphy of the Antarctic Margin II. Antarctic Research Series* 71. American Geophysical Union, Washington, pp. 169–187.
- Praeg, D.B., MacLean, B., Sonnichsen, G., 2007. *Quaternary Geology of the Northeast Baffin Island Continental Shelf, Cape Aston to Buchan Gulf (70° to 72°N)*. Geological Survey of Canada, Open File 5409.
- Prothro, L.O., Simkins, L.M., Majewski, W., Anderson, J.B., 2018. Glacial retreat patterns and processes determined from integrated sedimentology and geomorphology records. *Mar. Geol.* 395, 104–119.
- Rasmussen, S.O., Bigler, M., Blockley, S.P., Blunier, T., Buchardt, S.L., Clausen, H.B., Cvijanovic, I., Dahl-Jensen, D., Johnsen, S.J., Fischer, H., Gkinis, V., Guillec, M., Hoek, W.Z., Lowe, J.J., Pedro, J.B., Popp, T., Seierstad, I.K., Steffensen, J.P., Svensson, A.M., Valletonga, P., Vinther, B.M., Walker, M.J.C., Wheatley, J.J., Winstrup, M., 2014. A stratigraphic framework for abrupt climatic changes during the Last Glacial period based on three synchronized Greenland ice-core records: refining and extending the INTIMATE event stratigraphy. *Quat. Sci. Rev.* 106, 14–28.
- Rydningen, T.A., Vorren, T.O., Laberg, J.S., Kolstad, V., 2013. The marine-based NW Fennoscandian ice sheet: glacial and deglacial dynamics as reconstructed from submarine landforms. *Quat. Sci. Rev.* 68, 126–141.
- Sheldon, C., Jennings, A., Andrews, J.T., Cofaigh, C.Ó., Hogan, K., Dowdeswell, J.A., Seidenkrantz, M.S., 2016. Ice stream retreat following the LGM and onset of the west Greenland current in Uummannaq Trough, west Greenland. *Quat. Sci. Rev.* 147, 27–46.
- Simon, Q., Hillaire-Marcel, C., St-Onge, G., Andrews, J.T., 2014. North-eastern Laurentide, western Greenland and southern Innuitian ice stream dynamics during the last glacial cycle. *J. Quat. Sci.* 29, 14–26.
- Simon, Q., St-Onge, G., Hillaire-Marcel, C., 2012. Late Quaternary chronostratigraphic framework of deep Baffin Bay glaciomarine sediments from high-resolution paleomagnetic data. *G-cubed* 13, Q0A003.
- Slabon, P., Dorschel, B., Jokat, W., Myklebust, R., Hebbeln, D., Gebhardt, C., 2016. Greenland ice sheet retreat history in the northeast Baffin Bay based on high-resolution bathymetry. *Quat. Sci. Rev.* 154, 182–198.
- Spagnolo, M., Clark, C.D., Ely, J.C., Stokes, C.R., Anderson, J.B., Andreassen, K., Graham, A.G.C., King, E.C., 2014. Size, shape and spatial arrangement of mega-scale glacial lineations from a large and diverse dataset. *Earth Surf. Process. Landforms* 39 (11), 1432–1448.
- Stocker, T.F., Qin, D., Plattner, G.K., Tignor, M., Allen, S.K., Boschung, J., Nauels, A., Xia, Y., Bex, V., Midgley, P.M. (Eds.), 2013. *Climate Change 2013: the Physical Science Basis. Contribution of Working Group I to the Fifth Assessment Report of the Intergovernmental Panel on Climate Change*. Cambridge University Press, p. 1535.
- Stokes, C.R., Clark, C.D., 1999. Geomorphological criteria for identifying Pleistocene ice streams. *Ann. Glaciol.* 28, 67–74.
- Stokes, C.R., Clark, C.D., 2001. Palaeo-ice streams. *Quat. Sci. Rev.* 20, 1437–1457.
- Stokes, C.R., Clark, C.D., 2002. Ice stream shear margin moraines. *Earth Surf. Process. Landforms* 27, 547–558.
- Stokes, C.R., Tarasov, L., Dyke, A.S., 2012. Dynamics of the north American ice sheet complex during its inception and build-up to the last glacial maximum. *Quat. Sci. Rev.* 50, 86–104.
- Straneo, F., Hamilton, G.S., Sutherland, D.A., Stearns, L.A., Davidson, F., Hammill, M.O., Stenson, G.B., Rosing-Asvid, A., 2010. Rapid circulation of warm subtropical waters in a major glacial fjord in East Greenland. *Nat. Geosci.* 3 (3), 182–186.
- Streuff, K., Cofaigh, C.Ó., Noormets, R., Lloyd, J.M., 2017. Submarine landforms and glaciomarine sedimentary processes in Lomfjorden, East Spitsbergen. *Mar. Geol.* 390, 51–71.
- Streuff, K., Cofaigh, C.Ó., Noormets, R., Lloyd, J., 2018. Submarine landform assemblages and sedimentary processes in front of Spitsbergen tidewater glaciers. *Mar. Geol.* 402, 209–227.
- Syvitski, J.P., 1991. Towards an understanding of sediment deposition on glaciated continental shelves. *Continent. Shelf Res.* 11 (8–10), 897–937.
- Syvitski, J.P.M., Shaw, J., 1995. Sedimentology and geomorphology of fjords. In: Perillo, G.M.E. (Ed.), *Developments in Sedimentology*. Elsevier, Amsterdam, pp. 113–178.
- Syvitski, J., Andrews, J.T., Schafer, C.T., Stravers, J.A., 2022. Sediment fill of Baffin island fjords: architecture and rates. *Quat. Sci. Rev.* 284, 107474.
- Tang, C.C., Ross, C.K., Yao, T., Petrie, B., DeTracey, B.M., Dunlap, E., 2004. The circulation, water masses and sea-ice of Baffin Bay. *Prog. Oceanogr.* 63 (4), 183–228.
- Thomas, E.K., Szymanski, J., Briner, J.P., 2010. Holocene alpine glaciation inferred from lacustrine sediments on NE Baffin Island, Arctic Canada. *J. Quat. Sci.* 25 (2), 146–161.
- Tinto, K.J., Padman, L., Siddoway, C.S., Springer, S.R., Fricker, H.A., Das, I., Caratori Tontini, F., Porter, D.F., Frearson, N.P., Howard, S.L., Siegfried, M.R., Mosbeux, C., Becker, M.K., Beretinato, C., Boghosian, A., Brady, N., Burton, N.L., Chu, W.,

- Cordero, S.I., Dhakal, T., Dong, L., Gustafson, C.D., Keeshin, S., Locke, C., Lockett, A., O'Brien, G., Spergel, J.J., Starke, S.E., Tankersley, M., Wearing, M.G., Bell, R.E., 2019. Ross Ice Shelf response to climate driven by the tectonic imprint on seafloor bathymetry. *Nat. Geosci.* 12 (6), 441–449.
- Trottier, A.P., Lajeunesse, P., Gagnon-Poiré, A., Francus, P., 2020. Morphological signatures of deglaciation and postglacial sedimentary processes in a deep fjord-lake (Grand Lake, Labrador). *Earth Surf. Process. Landforms* 45 (4), 928–947.
- Tulaczyk, S., Scherer, R.P., Clark, C.D., 2001. A ploughing model for the origin of weak tills beneath ice streams: a qualitative treatment. *Quat. Int.* 86, 59–70.
- Vorren, T.O., Lebesbye, E., Andreassen, K., Larsen, K.B., 1989. Glacigenic sediments on a passive continental margin as exemplified by the Barents Sea. *Mar. Geol.* 85 (2–4), 251–272.
- Weertman, J., 1974. Stability of the junction of an ice sheet and an ice shelf. *J. Glaciol.* 13 (67), 3–11.
- Winsborrow, M.C., Andreassen, K., Corner, G.D., Laberg, J.S., 2010. Deglaciation of a marine-based ice sheet: late Weichselian palaeo-ice dynamics and retreat in the southern Barents Sea reconstructed from onshore and offshore glacial geomorphology. *Quat. Sci. Rev.* 29 (3), 424–442.
- Wise, M.G., Dowdeswell, J.A., Jakobsson, M., Larter, R.D., 2017. Evidence of marine ice-cliff instability in Pine Island Bay from iceberg-keel plough marks. *Nature* 550 (7677), 506–510.
- Woodworth-Lynas, C.M.T., Josenhans, H.W., Barrie, J.V., Lewis, C.F.M., Parrott, D.R., 1991. The physical processes of seabed disturbance during iceberg grounding and scouring. *Continent. Shelf Res.* 11 (8–10), 939–961.
- Young, N.E., Briner, J.P., Rood, D.H., Finkel, R.C., 2012. Glacier extent during the younger Dryas and 8.2-ka event on Baffin island, arctic Canada. *Science* 337, 1330–1333.
- Young, N.E., Schaefer, J.M., Briner, J.P., Goehring, B.M., 2013. A ^{10}Be production-rate calibration for the Arctic. *J. Quat. Sci.* 28 (5), 515–526.
- Young, N.E., Schweinsberg, A.D., Briner, J.P., Schaefer, J.M., 2015. Glacier maxima in Baffin bay during the medieval warm period coeval with norse settlement. *Sci. Adv.* 1 (11), e1500806.
- Young, N.E., Briner, J.P., Miller, G.H., Lesnek, A.J., Crump, S.E., Thomas, E.K., Pendleton, S.L., Cuzzone, J., Lamp, J., Zimmerman, S., Caffe, M., Schaefer, J.M., 2020. Deglaciation of the Greenland and Laurentide ice sheets interrupted by glacier advance during abrupt coolings. *Quat. Sci. Rev.* 229, 106091.
- Young, N.E., Briner, J.P., Miller, G.H., Lesnek, A.J., Crump, S.E., Pendleton, S.L., Schwartz, R., Schaefer, J.M., 2021. Pulsebeat of early Holocene glaciation in Baffin Bay from high-resolution beryllium-10 moraine chronologies. *Quat. Sci. Rev.* 270, 107179.